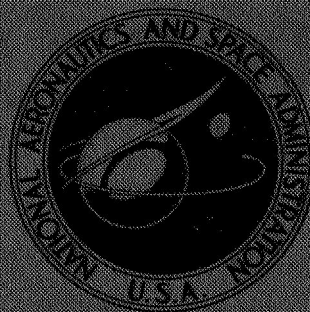


NASA TECHNICAL
MEMORANDUM



NASA TM X-1414

NASA TM X-1414

FACILITY FORM 802

N67-32265
(ACCESSION NUMBER)

45
(PAGES)

TMX-1414
(NASA CR OR TMX OR AD NUMBER)

1
(THRU)

01
(CODE)

~~01~~
(CATEGORY)

FLIGHT TEST OF A 31.2-FOOT-DIAMETER
MODIFIED RINGSAIL PARACHUTE
DEPLOYED AT A MACH NUMBER OF 1.39
AND A DYNAMIC PRESSURE
OF 11.0 POUNDS PER SQUARE FOOT

*by John S. Preisser, Clinton V. Eckstrom,
and Harold N. Murrow*

*Langley Research Center
Langley Station, Hampton, Va.*

GPO PRICE \$ _____

CFSTI PRICE(S) \$ 3.00

Hard copy (HC) _____

Microfiche (MF) 65

ff 653 July 65

**FLIGHT TEST OF A 31.2-FOOT-DIAMETER
MODIFIED RINGSAIL PARACHUTE DEPLOYED AT A
MACH NUMBER OF 1.39 AND A DYNAMIC PRESSURE
OF 11.0 POUNDS PER SQUARE FOOT**

**By John S. Preisser, Clinton V. Eckstrom,
and Harold N. Murrow**

**Langley Research Center
Langley Station, Hampton, Va.**

Technical Film Supplement L-966 available on request.

NATIONAL AERONAUTICS AND SPACE ADMINISTRATION

**For sale by the Clearinghouse for Federal Scientific and Technical Information
Springfield, Virginia 22151 - CFSTI price \$3.00**

FLIGHT TEST OF A 31.2-FOOT-DIAMETER
MODIFIED RINGSAIL PARACHUTE DEPLOYED AT A
MACH NUMBER OF 1.39 AND A DYNAMIC PRESSURE
OF 11.0 POUNDS PER SQUARE FOOT

By John S. Preisser, Clinton V. Eckstrom,
and Harold N. Murrow
Langley Research Center

SUMMARY

A 31.2-foot (9.51 meter) nominal diameter (reference area 764 ft² (71.0 m²)) ring-sail parachute modified to provide 15-percent geometric porosity was flight tested while attached to a 201-pound mass (91.2 kilogram) instrumented payload as part of the rocket launch portion of the NASA Planetary Entry Parachute Program (PEPP). The parachute deployment was initiated by the firing of a mortar at a Mach number of 1.39 and a dynamic pressure of 11.0 lb/ft² (527 N/m²) at an altitude of 122 500 feet (37.3 kilometers). The parachute deployed to suspension-line stretch (snatch force) in **0.35** second, and 0.12 second later the drag force increase associated with parachute inflation began. The parachute inflated in 0.24 second to the full-open condition for a total elapsed opening time of 0.71 second. The maximum opening load of **3970** pounds (17 700 newtons) came at the time the parachute was just fully opened. During the deceleration period, the parachute exhibited an average drag coefficient of 0.52 and oscillations of the parachute canopy were less than 5°. During the steady-state terminal descent portion of the test period, the average effective drag coefficient (based on vertical descent velocity) was 0.52.

INTRODUCTION

The NASA Planetary Entry Parachute Program (PEPP) was established to provide test data on several parachute configurations for applications in low-density environments (ref. 1). The Voyager program, for example, has immediate requirements for such data. The ringsail parachute, which was one of the configurations selected to be tested in the program, was originally developed for and has been used extensively in payload recovery operations. Development testing has included wind-tunnel tests of models and drop tests of full-scale units from aircraft. In addition to being lightweight, the ringsail parachute was found to have good drag capabilities and exhibited relatively

good stability in the subsonic Mach number range for which it was designed. The parachute was designed to provide minimum opening loads, and in addition, on most of the previous applications, it was reefed during the deployment process to reduce opening loads further. Probably, the most well-known application of the ringsail parachute has been in the recovery of manned spacecraft.

The flight-test conditions of interest are deployment at low supersonic Mach numbers combined with low dynamic pressures which can be achieved at earth altitudes above 100,000 feet (30.5 kilometers). An earlier test in the program was made of an 85.3-foot (26 meter) ringsail parachute deployed in a reefed condition at a Mach number of 1.15 and at an altitude of 132 600 feet (40.4 kilometers) (ref. 2). The deployment conditions selected for the flight test reported herein were a Mach number of 1.6 and a dynamic pressure of 10 lb/ft^2 (479 N/m^2) and the test parachute was a 31.2-foot (9.51 meter) modified ringsail parachute. The parachute was deployed unreefed and the test objectives were to observe the dynamics of parachute deployment and inflation and to measure opening shock loads, parachute drag, and stability characteristics. The test was made by utilizing the rocket-launch method originally discussed in reference 1.

A motion picture film supplement is available on loan. The film shows deployment, inflation, and the flight configuration as taken from a camera onboard the payload.

SYMBOLS

a_X, a_Y, a_Z	accelerations relative to center of gravity of payload parallel to missile X-, Y-, and Z-axes, respectively, ft/sec^2 (m/sec^2)
a_l, a_n, a_t	accelerations measured by onboard accelerometers, g units (Refer to sketch (3) in appendix)
$C_{D,o}$	drag coefficient
$(C_{D,o})_{\text{eff}}$	effective drag coefficient (based on vertical descent velocity)
D	drag force, lb (N)
D_o	nominal diameter, $\left(\frac{4}{\pi} S_o\right)^{1/2}$, ft (m)
g	acceleration due to gravity, ft/sec^2 (m/sec^2)
M	Mach number
q_∞	free-stream dynamic pressure, lb/ft^2 (N/m^2)

S_0	nominal surface area of parachute canopy including all openings such as slots and vents, ft ² (m ²)
t	time from vehicle lift-off, sec
t'	time from mortar firing, sec
W	weight, lbm (kg)
X, Y, Z	body axis system (refer to sketch (1) in appendix)
X_u, Y_u, Z_u	body axis system at time of gyro uncaging (inertial coordinate system)
$\Delta X, \Delta Y, \Delta Z$	distance between payload center-of-gravity and accelerometer locations along X-, Y-, and Z-axes, respectively, ft (m)
Z_E	local vertical
δg	resultant pitch-yaw oscillation angle of payload about its mean pitch-yaw attitude (Refer to sketch (2) in appendix)
θ_g, ψ_g, ϕ_g	gyro angles defining payload body axis system relative to inertial coordinate system
ρ_∞	free-stream atmospheric density, slugs/ft ³ (kg/m ³)
$\omega_X, \omega_Y, \omega_Z$	angular velocities about X-, Y-, and Z-axes, respectively, radians/sec

Dots over symbols denote differentiation with respect to time. Bars over symbols denote average or mean values.

TEST SYSTEM DESCRIPTION

A photograph of the vehicle configuration used is presented in figure 1. The payload containing the test parachute was launched by an Honest John—Nike rocket system. The Nike fins were canted to impart a stabilizing spin to the system. Payload separation from the second stage was effected by a pressurized bellows which provided a separation velocity of 30 feet per second (9 meters per second). Six small rocket motors were mounted in the ballast section perpendicular to the longitudinal axis of the vehicle and fired immediately after payload separation to provide a tumbling motion to the spent

Nike booster and to prevent possible impact with the parachute after deployment. The weight of the ballast section was such that the payload would have the proper velocity at the test altitude. A diagram of the instrumented payload from which the test parachute was deployed is shown in figure 2. Note that the payload contained two backup or recovery parachutes which could be deployed if the test parachute failed to deploy or was damaged to such an extent that the projected impact velocity would be great. In addition to the data-gathering instrumentation, two beacons were installed in the payload as a tracking aid for the recovery aircraft. The weight of the instrumented payload was approximately 201 pounds mass (91.2 kilograms); total descent weight including the test parachute was approximately 221 pounds mass (100.2 kilograms).

Payload Instrumentation

The data-acquisition instrumentation on board the payload consisted of a tensiometer, three orthogonally mounted accelerometers, an attitude reference system, and two cameras.

The tensiometer, which employed a strain gage, was placed in the parachute riser line to measure the force exerted on the payload by the test parachute. The tensiometer was scaled from 0 to 10 000 lb (44 800 N) and the maximum intelligible frequency of data was 1050 cps.

Accelerations of the payload were measured by servo accelerometers using a capacitance sensor. One of the accelerometers was aligned with the longitudinal axis of the payload, was ranged to $\pm 75g$ units, and had a flat frequency-response curve up to 500 cps. The other two accelerometers were mounted normal to the payload longitudinal axis and normal to each other. These normal accelerometers were ranged to $\pm 5g$ units and had flat frequency response up to 100 cps. All three accelerometers were installed forward of the center of mass of the payload. (See table in the appendix.)

The attitude reference system, hereafter referred to as a gyro platform, consisted of two two-degree-of-freedom gyros mounted on a common gimbal. The gyro platform measured the attitude of the payload during flight relative to an inertial reference.

One of the payload cameras was pointed aft to record parachute deployment, inflation, and overall operation. The aft camera frame rate was set at 64 frames per second. The second camera was mounted in the nose of the payload looking forward, had its frame rate set at 16 frames per second, and was located to provide data on payload motions relative to earth during the flight test.

The tensiometer, accelerometer, and gyro platform data were telemetered to ground recording stations. Recovery of the payload was required to obtain the camera film. Coded timing appeared on both film data and the telemetry records.

Command Deployment Description

A radio command system was used to start the onboard cameras and a programmer. The programmer initiated the firing of the parachute deployment mortar 1 second after the command was received in order to allow the cameras to reach full speed. A visual display derived from radar data, such as is shown in figure 3, was used to determine the proper time for initiation of the radio command signal. Mach number and dynamic pressure grids were prepared for the region of anticipated parachute deployment based on recent meteorological data and were plotted, prior to flight, as functions of altitude and velocity on the radar display. Position data for the vehicle in flight were obtained by tracking with FPS-16 radars. The tracking accuracy was enhanced by means of a C-band transponder in the payload. The position data were processed by a digital computer programmed to compute altitude (mean sea level) and velocity relative to earth. The results of this operation were presented in real time by means of a time updating technique. Variation of altitude with velocity was presented on the plotboard display by means of an X,Y plotter. The attempt was made to transmit the radio command signal such that parachute deployment would occur as closely as possible to the planned combination of a Mach number of 1.6 and a dynamic pressure of 10 psf (479 N/m^2). It was recognized in advance that deviations from the nominal flight path would cause deployment to vary by some amount from the nominal test conditions.

The command system could also be used to deploy the backup parachutes at any time after payload separation from the Nike if they were needed.

TEST PARACHUTE DESCRIPTION

The test parachute was a ringsail design modified to provide 15-percent geometric porosity or open area. The test parachute had a reference area of 764 square feet (71.0 square meters) and a nominal diameter D_0 of 31.2 feet (9.51 meters). The ringsail parachute was constructed with 24 suspension lines and 24 gores with 10 panels in each gore. The upper 3 panels, which are separated by slots, are called rings, and the lower 6 panels are referred to as sails. The major modification was the removal of the eighth panel in each gore in order to achieve the desired porosity. Figure 4 presents the dimensional details of a gore (supplied by the manufacturer) and the general parachute payload configuration. The in-flight projected diameter of the ringsail parachute was approximately 21 feet (6.4 meters).

The test parachute was fabricated in its entirety of dacron materials. The canopy sails were fabricated from 1.9 ounce per square yard (65 gram per square meter) dacron cloth of plain weave. The material was originally 1.8 ounce per square yard (61 gram per square meter) but had been subjected to a heat-setting treatment before fabrication which caused the material to shrink. The upper edge of panel 1 (the vent edge) was

reinforced with a $3/4$ -inch (1.9-centimeter) wide 550-pound (2450-newton) tensile strength dacron tape. The upper edges of panels 2 and 3 in each gore were reinforced with a similar tape but of 300-pound (1330-newton) tensile strength. The upper edges of panels 4 to 10 in each gore were unreinforced except for the selvedge edge of the material. The lower edges of all panels were reinforced with a $1/2$ -inch (1.3-centimeter) wide rolled hem. The lower edge of panel 10, the canopy skirt, was further reinforced with a dacron tape having a 550-pound (2450-newton) tensile strength. The panels in each ring were first joined at the gore edges by a $3/4$ -inch (1.9-centimeter) wide French fell seam. The panel rings were then joined to form the canopy by a $3/4$ -inch (1.9-centimeter) wide gore tape of 550-pound (2450-newton) tensile strength dacron. The suspension lines, which were 30 feet (9 meters) long, and the vent lines were coreless braided dacron having a tensile strength of 300 pounds (1330 newtons).

The parachute attachment system consisted of a riser, a tensiometer, and a bridle. The riser was 4 feet (1.2 meters) in length and the tensiometer was approximately $1/2$ foot (0.15 meters) long. The bridle consisted of a single line for $1\frac{1}{2}$ feet (0.45 meters); this line then separated into three legs, each of which was 3 feet (0.91 meters) long, and thus provided a three-point attachment to the payload. The riser consisted of two layers of $1\frac{3}{4}$ -inch (3.3-centimeters) wide low elongation dacron webbing of 7000-pound (31 100-newton) tensile strength. The single line of the bridle also was two layers of 7000-pound (31 100-newton) webbing. Each leg of the bridle was a single thickness of 7000-pound (31 100-newton) webbing.

The weight of the test parachute including the riser was 19.8 pounds mass (9.0 kilograms). The parachute was pressure packed to a density of 40 pounds mass per cubic foot (641 kilograms per cubic meter) in a cylindrical dacron bag which was closed with a bag mouth tie. No canopy or suspension line holders or restraints were used inside the deployment bag except for a break line from the apex of the canopy to the bottom of the bag. The bag was lined with cotton cloth to prevent friction burning during packing and deployment.

The packed parachute was inserted into an oven and subjected to a temperature of 125° C for 120 hours. This heat cycle is representative of part of the sterilization requirements for equipment to be used in interplanetary spacecraft. The packed parachute and deployment bag were subjected to the heat cycle so that any degradation of material strength or elastic properties or any deployment problems which may result from spacecraft heat sterilization would exist during the flight test.

The test parachute was ejected from the aft end of the payload by means of a deployment mortar which was approximately 12 inches (30.5 centimeters) in diameter and 17 inches (43.2 centimeters) in length. The mortar was designed to eject the packed parachute at an initial velocity of 120 feet per second (36.6 meters per second). The

mouth of the deployment bag was inserted in the mortar first and rested on the sabot (deployment piston) at the bottom of the mortar. The mortar cover, which was fastened to the bottom of the deployment bag, closed the mortar and held the packed parachute in place. A circular knife located on the parachute riser was used to cut the deployment bag mouth tie after the bag was ejected from the spacecraft. The test parachute was packed so that the suspension lines deployed first and then the canopy. When the suspension lines were fully extended, the combined inertia of the mortar cover and the deployment bag were used to extract the parachute canopy (no pilot parachute was used).

The test parachute was equipped with a system of lines which allowed it to be reefed after the parachute test period was completed. Since the parachute was not reefed at any time during the actual test, the system of lines was termed a "post-reefing" system. Post-reefing was used to increase parachute descent rate, and thereby reduce total flight time and the corresponding parachute drift due to winds.

RESULTS AND DISCUSSION

Test Data

The flight test vehicle was launched at 6:45 a.m. m.s.t. on November 24, 1966, at White Sands Missile Range, New Mexico. The flight sequence is shown in figure 5 and the recorded event times are listed on the right-hand side of the figure. Time histories of the altitude and relative velocity from lift-off through the parachute test period are shown in figure 6.

A meteorological sounding rocket was launched 1 hour after the flight test to measure upper altitude winds and temperatures. This information was supplemented by a rawinsonde at 1 hour and 35 minutes after the flight test. Upper atmospheric winds as determined from the sounding rocket are presented in figure 7. Temperature information is presented in figure 8 for the rawinsonde and the rocket soundings. Atmospheric density, derived from temperature data by the method in reference 3, is presented in figure 9.

The measured atmospheric properties were used with radar track and telemetered data to determine the payload true airspeed, Mach number, and dynamic pressure (figs. 10 and 11) during the deployment period. The initiation of the deployment sequence or time of deployment is defined by mortar firing (labeled $t' = 0$ on figures). As indicated in figures 10 and 11, the parachute deployment was initiated at a true airspeed of 1405 fps (428 mps) ($M = 1.39$) and a dynamic pressure of 11.0 psf (527 N/m^2). By using a first-order error analysis, uncertainties in the deployment conditions were calculated to be ± 0.02 for Mach number and ± 0.4 psf ($\pm 19 \text{ N/m}^2$) for dynamic pressure, based on 1-percent velocity error, 2-percent temperature error, and 3-percent density error.

The true airspeed and Mach number data presented in figure 10 are based on radar tracking up to the instant the deployment mortar was fired. From the time of mortar firing to $t' = 6$ seconds, true airspeed was determined from integrated tensiometer data which was essentially identical with that determined from integrated accelerometer data. Radar track data yielded different results during the initial deployment period as it had been subjected to a data filtering process. Within 2.0 seconds after the deployment mortar fired, the velocity established by integration of both sets of telemetered data was in good agreement with the radar track data.

The payload velocity increased slightly immediately after initiation of the deployment sequence as shown in figure 10 because of the reaction on the payload caused by firing the mortar. A slight decrease in velocity at $t' = 0.35$ second was associated with the snatch-force loads which occurred when the parachute suspension lines were deployed full length. A rapid decrease in velocity occurs at $t' = 0.7$ to 0.8 second when the parachute is first fully opened. The system velocity decreased approximately 50 percent (from 1405 fps (428 mps) to 700 fps (213 mps)) within 2.7 seconds after deployment was initiated. The minimum true airspeed was 182 feet per second (55 meters per second), which occurred at apogee, $t' = 12$ seconds. The altitude of the parachute-payload system during the deployment sequence, as determined by radar tracking, is presented in figure 12. Note that parachute deployment was initiated at an altitude of 122 500 feet (37.3 kilometers) while the payload was ascending and apogee occurred at 126 600 feet (38.6 kilometers).

The time history of forces transmitted through the riser line as measured by the tensiometer during the deployment period is presented in figure 13. The first peak force of 560 pounds (2440 newtons) occurred when the parachute attachment bridle and riser were deployed full length. This force occurred 0.15 second after the deployment mortar fired. The second peak force of 1700 pounds (7560 newtons) occurred at line stretch, $t' = 0.35$ second. The maximum force of 3970 pounds (17 700 newtons) was recorded at $t' = 0.71$ second. This time is the instant the parachute was first fully opened as determined from the aft camera film. The tensiometer force decreased rapidly to 2520 pounds (11 200 newtons) at 0.98 second after which there was an increase in force to 2890 pounds (12 800 newtons) at $t' = 1.05$ seconds. Thereafter, the tensiometer force decreased gradually to 250 pounds (1100 newtons) at 6 seconds.

Figure 14 presents the data obtained from the three orthogonally mounted accelerometers in the payload. The data are presented for a 6-second period beginning with the time of mortar firing. For convenience with regard to scaling on the figure, the positive longitudinal accelerations imposed by the firing of the mortar are not shown. (Mortar firing provided an average acceleration of 20g units to the payload over a 0.02-second period.) Note that the shape of the longitudinal accelerometer time history is similar

to that contained in figure 13 for the tensiometer. A deceleration of 2g was recorded at $t' = 0.15$ second and a deceleration of 6.5g at $t' = 0.35$ second. These two peak decelerations correspond to peaks noted on the tensiometer record and, as mentioned previously, are attributed to riser deployment and suspension line stretch. The maximum shock of 20g occurred at $t' = 0.71$ second and corresponded to full opening of the parachute. The deceleration dropped to approximately 1.0g by $t' = 6$ seconds.

Time histories of accelerations recorded by the two accelerometers mounted normal to the longitudinal axis of the payload (fig. 14) indicate that the payload did not remain in line with the flight path; this result was confirmed by the gyro data together with the aft camera film. Therefore, in addition to the deceleration of the center of mass of the payload, the three accelerometers which were not located at the center of mass of the payload also contained accelerations due to payload motions in pitch, yaw, and roll. Components along the body axis of those accelerations due to angular motions of the payload were calculated by the method outlined in the appendix and subtracted from the accelerometer data to obtain a total deceleration of the center of mass. This deceleration of the center of gravity of the payload was caused directly by the parachute drag forces. For this flight test, the contribution of pitch, yaw, and roll to the longitudinal accelerometer measurements was in the range of from 0 to approximately 0.5g (0 to approximately 10 percent). Of course, most of the recorded data for the normal and transverse accelerometers was caused by this pitch, yaw, and roll motion of the payload.

Payload motions in pitch, yaw, and roll were measured by the gyro platform. These angles were measured relative to the fixed position of the vehicle on the launcher at lift-off since this was the position at the time the gyro platform was uncaged. The physical construction of the platform determined the definition of the measured angles. These angles are Euler angles in the sequence: pitch, θ_g ; yaw, ψ_g ; roll, ϕ_g . The gyro platform transformation from space coordinates, determined by the uncaged position, to payload body axis coordinates during flight is given in the appendix. Time histories of pitch and yaw for the payload after mortar fire are shown in figure 15. Note that both pitch and yaw show a generally increasing trend with a superimposed oscillation. The general increase in magnitude in pitch, labeled $\bar{\theta}_g$ in figure 15, is due to the normal system pitch-down as apogee is approached. It is to be noted that the buildup in yaw $\bar{\psi}_g$ resulted from the system velocity being comparable in magnitude to the wind velocity near apogee and approximately normal to it so that the payload-parachute combination turned into the direction of relative airflow. Comparison of the oscillatory portion of the pitch and yaw time histories in magnitude, frequency, and phase indicates payload precession was induced by the parachute drag force on the spinning payload as would be expected. At $t' = 13.4$ seconds, the total yaw angle reached -850° ; at this point the gyro has mechanical stops. The platform therefore tumbled and the inertial reference was lost; as a result, gyro data were not available for the remainder of the test.

Payload roll rate at the time of parachute deployment was 5.0 cycles per second. This rate rapidly decreased as the bridle and riser system absorbed roll energy by winding up. At $t' = 7$ seconds, the roll rate had decreased to 1 cycle per second. During the parachute test period, the payload went through several roll oscillations characterized by a series of payload windings and unwindings beneath the parachute.

Film data were obtained from the aft-looking camera for a period of approximately 50 seconds at a rate of 64 frames per second. These film data provided parachute roll motions relative to the payload, as well as a time history of the resultant pitch-yaw angle between the parachute and the payload.

The accuracy of the data obtained from the tensiometer, accelerometers; and gyro platform is a function of the uncertainties in the respective instruments, the telemetry system, the magnetic tape recording, and the data reduction process. Instrument errors of 0.2 percent for the tensiometer and 0.5 percent for the accelerometers, in addition to an estimated 0.5 percent uncertainty in telemetry, recording, and data reduction, result in uncertainties of ± 50 pounds (220 newtons) in the tensiometer data and $\pm 0.5g$ for the longitudinal accelerometer data. A detailed error analysis based on unpublished data at Langley Research Center was made for the gyro platform. Results of this analysis showed uncertainties in pitch, yaw, and roll to be $\pm 1.5^\circ$, $\pm 1.1^\circ$, and $\pm 1.6^\circ$, respectively, during the parachute deployment and deceleration phase.

Parachute Performance

Inflation characteristics. - The parachute deployed to suspension line stretch in 0.35 seconds after the mortar fired. The average deployment velocity was 111 ft/sec (33.8 m/sec) with a resulting snatch force of 1700 pounds (7560 newtons).

The increase in drag force associated with parachute inflation began 0.12 seconds after line stretch. The parachute was fully open 0.24 second later for a total elapsed time from mortar fire to full inflation of 0.71 second. The "opening shock," which is the maximum drag force created by the parachute during the opening process, was 3970 pounds (17 700 newtons). This maximum load occurred at the time the parachute was first fully opened. Thereafter the system decelerated rapidly as the equilibrium canopy area loading (W/S_0) was low (approximately 0.29 lb/ft² (13.9 N/m²)) and the drag loads decreased correspondingly.

Several frames of the aft camera film showing canopy inflation are presented in figure 16(a). The aft camera film revealed that the parachute skirt fluttered slightly immediately after opening as shown in figure 16(b). The short unsteady period of canopy shape variation is attributed to the rapidly changing flow pattern in the region of the parachute canopy during inflation and immediately after the canopy was first fully opened. The fully inflated parachute is shown in figure 16(c).

Drag efficiency.- As noted earlier, the payload was at a Mach number of **1.39** when the deployment mortar fired and at a Mach number of **1.32** when the parachute was first fully opened. The system decelerated to subsonic velocities in less than 0.6 second after the parachute was first fully opened or **1.3** seconds from the time the deployment mortar fired. The computed drag coefficient $C_{D,o}$ for the parachute is presented in figure 17 as a function of Mach number during the deceleration period immediately after deployment. The parachute, which had a total canopy area of **764** square feet (**71.0** square meters), had an average $C_{D,o}$ of about **0.52** during this period. Drag forces were calculated from both the recorded tensiometer force data and the calculated center-of-gravity deceleration of the payload. Since the parachute was decelerating the total system rather than just the payload, the total drag force was larger than the recorded tensiometer force by the ratio of the total system weight to the payload weight (**1.1:1.0**). The equation used to determine the drag coefficient is as follows:

$$C_{D,o} = \frac{D}{q_{\infty} S_o}$$

As the percent error in accelerometer and tensiometer data increased with time from mortar fire, the uncertainty in $C_{D,o}$ increased from ± 0.03 at **0.7** second to ± 0.15 at **5.0** seconds. From **5.0** to **10.0** seconds, radar track data were used to derive $C_{D,o}$ values, since the estimated uncertainty was calculated to be ± 0.12 . Uncertainties in $C_{D,o}$ are based on a first-order error analysis using uncertainties in the measured quantities mentioned previously. Payload drag was very small compared with the parachute drag and was neglected in the calculations.

Figure 18 presents the vertical descent velocity and "effective" drag coefficient variations with altitude. The effective drag coefficient values are based on steady-state or equilibrium vertical-descent velocities and the system weight as shown by the following equation:

$$(C_{D,o})_{\text{eff}} = \frac{2W}{\rho_{\infty} \dot{Z}_E^2 S_o}$$

The start of steady-state descent was taken to be the time at which the deceleration of the system became less than 0.1g. Based on radar track data, this time corresponded to an altitude of **115 000** feet (**35.0** kilometers). During steady-state descent, the average effective drag coefficient was about **0.52**. The average uncertainty in $(C_{D,o})_{\text{eff}}$ based on a 3-percent density error and a 7-percent vertical velocity error, was calculated to be ± 0.05 . The slight increase in velocity which occurred at **76 000** feet (**23.1** kilometers) altitude resulted from the parachute post-reefing function.

Stability.- As mentioned previously, the gyro platform gave a measure of the payload attitude with respect to an inertial reference. The payload camera focused on the test parachute provided data on relative motions and angular displacements between the payload and the parachute. A comparison of the relative payload-parachute roll rate as measured from the camera film with the payload roll rate from gyro platform data is given in figure 19 for a 12-second period subsequent to mortar fire. The difference between these data represents the roll motion of the parachute canopy. Note that at 1 second after mortar fire, the parachute canopy had built up a rolling motion on the order of 0.5 radian per second in a direction opposite to the roll of the payload. This motion was confirmed by analyzing the position of a canopy gore relative to the sun from camera film data. It is believed that canopy shape variations which occurred after the parachute was first fully opened (refer to fig. 16(b)) induced this canopy roll.

A time history of the relative pitch-yaw angle between the parachute and the payload as determined from the camera film is presented in figure 20 along with the resultant pitch-yaw payload oscillation angle δ_g computed from gyro data. Note the direct agreement to within 5° between the camera data and the gyro platform data during the 5-second period immediately after mortar fire. This time period, as shown previously, corresponded to the major deceleration period of the system. From this comparison, it is concluded that parachute stability represented by the difference between δ_g and the film data angle was good during the system deceleration period. The difference between parachute-payload and payload pitch-yaw oscillations becomes as high as 12° from $t' = 5$ seconds to $t' = 12$ seconds. However, some disagreement can be expected during this latter time period, since high-altitude wind effects are greater on the parachute canopy when the system velocity is less.

Data on parachute stability during terminal descent was unavailable from this test because of the loss of gyro data, underexposure of the nose camera film, and the lack of any long-range telescopic camera coverage.

Analysis of recovered parachute.- The test parachute suffered some minor damage during deployment. The maximum damage as shown in figure 21 was to gore 23, sail 6, which was torn for 8 inches from the upper edge and along a gore tape. This damaged area is visible in the aft camera movie films as shown in figure 16(c). The canopy cloth was torn for lengths of less than 2 inches in seven other places; however, this additional damage is not noticeable in the film records.

Examination of the recovered parachute shown in figure 22 revealed that the folds placed in the parachute canopy during the packing operation were permanently pressed into the material during the heat cycle. It was also noted that the canopy was discolored in several places, possibly as a result of contact with the cotton liner in the deployment

bag. The discoloration and folds in the canopy material are not considered to have contributed to the aforementioned damage.

CONCLUDING REMARKS

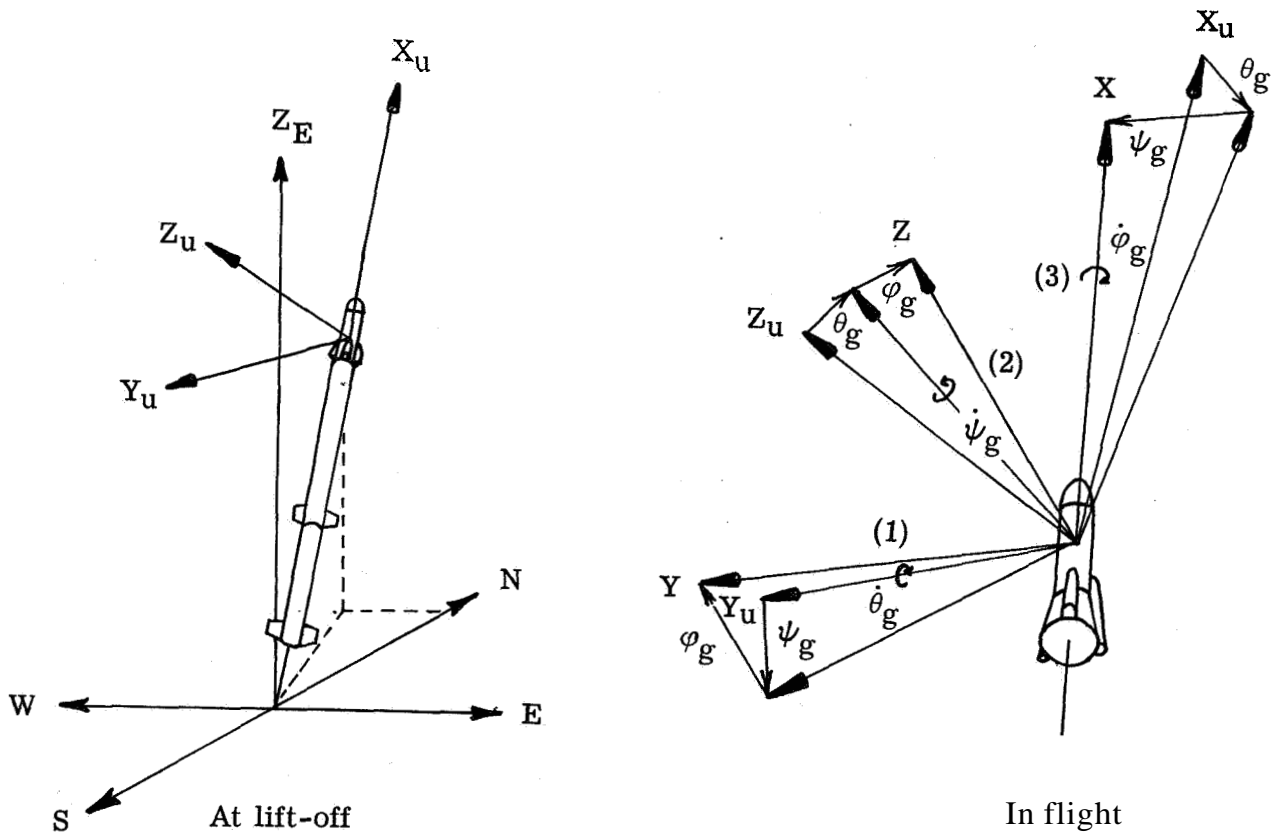
The 31.2-foot (9.51-meter) diameter modified ringsail parachute was tested by means of a two-stage rocket system and ejected from the payload by the firing of a mortar at a Mach number of 1.39 and a dynamic pressure of 11 psf (527 N/m²). The parachute deployed to suspension line stretch in 0.35 second and the corresponding snatch force was 1700 pounds (7560 newtons). The increase in drag force associated with parachute inflation began 0.12 second after line stretch and ended 0.24 second later at full inflation. The maximum opening shock occurred at full inflation and was 3970 pounds (17 700 newtons). The parachute exhibited good stability characteristics during the deceleration period; roll motion was approximately 0.5 radian/sec and pitch-yaw oscillations were less than 5°.

Langley Research Center,
National Aeronautics and Space Administration,
Langley Station, Hampton, Va., June 26, 1967,
709-08-00-01-23.

APPENDIX

NOTES ON INTERPRETATION OF GYRO PLATFORM DATA

The orientation of one coordinate system with respect to a second coordinate system can be completely specified by three Euler angles. The gyro platform provides a measure of three such angles so that the attitude of the payload, relative to an inertial coordinate system determined by the uncaged position of the platform on the launcher, can be determined at any time during the flight. The set of rotations which relate the body-axis system to the inertial coordinate system, as determined by platform construction, are in the order: (1) pitch, (2) yaw, and (3) roll. This relationship is shown in the following sketch:



Sketch (1)

where the origin is fixed at the center of mass of the payload and

X, Y, Z body-fixed axes

X_u, Y_u, Z_u inertial coordinate system (gyro uncaged axes)

APPENDIX

Z_E local vertical

$\theta_g, \psi_g, \varphi_g$ pitch, yaw, and roll angles, respectively

(Note that a right-handed coordinate system was used and the positive sense of the angles are shown in sketch (1); for example, pitch down is positive.)

The transformation equations relating the body-fixed axis to the inertial reference is

$$\begin{Bmatrix} X \\ Y \\ Z \end{Bmatrix} = \begin{bmatrix} 1 & 0 & 0 \\ 0 & \cos \varphi_g & \sin \varphi_g \\ 0 & -\sin \varphi_g & \cos \varphi_g \end{bmatrix} \begin{bmatrix} \cos \psi_g & \sin \psi_g & 0 \\ -\sin \psi_g & \cos \psi_g & 0 \\ 0 & 0 & 1 \end{bmatrix} \begin{bmatrix} \cos \theta_g & 0 & -\sin \theta_g \\ 0 & 1 & 0 \\ \sin \theta_g & 0 & \cos \theta_g \end{bmatrix} \begin{Bmatrix} X_u \\ Y_u \\ Z_u \end{Bmatrix} \quad (A1)$$

and it follows that

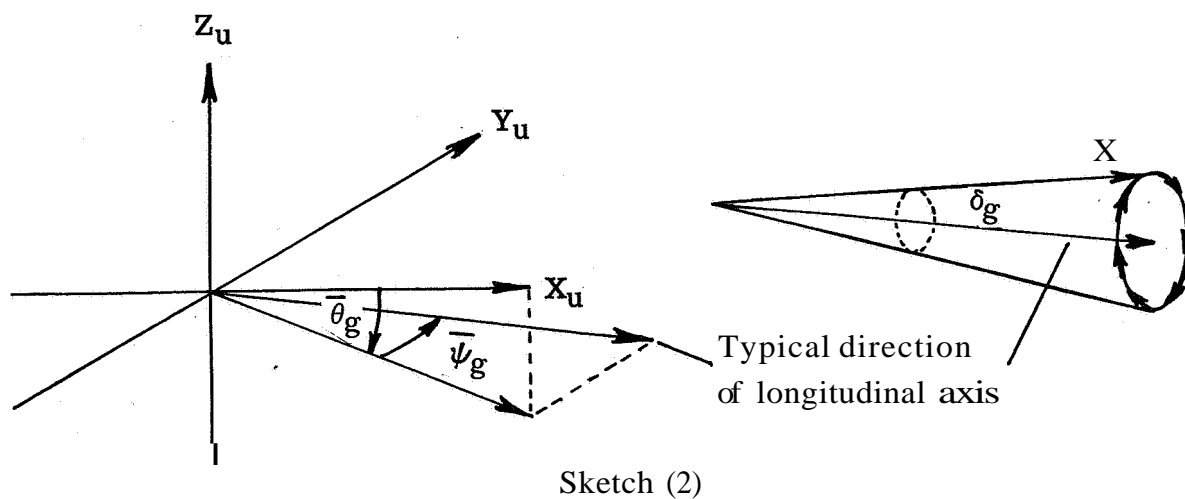
$$\begin{Bmatrix} X \\ Y \\ Z \end{Bmatrix} = \begin{bmatrix} \cos \psi_g \cos \theta_g & \sin \psi_g & -\cos \psi_g \sin \theta_g \\ -\cos \varphi_g \sin \psi_g \cos \theta_g & \cos \psi_g \cos \varphi_g & \cos \varphi_g \sin \psi_g \sin \theta_g \\ + \sin \varphi_g \sin \theta_g & & + \sin \varphi_g \cos \theta_g \\ \sin \varphi_g \sin \psi_g \cos \theta_g & -\sin \varphi_g \cos \psi_g & -\sin \varphi_g \sin \psi_g \sin \theta_g \\ + \cos \varphi_g \sin \theta_g & & + \cos \varphi_g \cos \theta_g \end{bmatrix} \begin{Bmatrix} X_u \\ Y_u \\ Z_u \end{Bmatrix} \quad (A2)$$

Components of the angular velocity vector along the body-axis system can be expressed in terms of the gyro angles as follows:

$$\left. \begin{aligned} \omega_X &= (\sin \psi_g) \dot{\theta}_g + \dot{\varphi}_g \\ \omega_Y &= (\cos \psi_g \cos \varphi_g) \dot{\theta}_g + (\sin \varphi_g) \dot{\psi}_g \\ \omega_Z &= -(\cos \psi_g \sin \varphi_g) \dot{\theta}_g + (\cos \varphi_g) \dot{\psi}_g \end{aligned} \right\} \quad (A3)$$

Note that these gyro angles include the slowly varying pitch and yaw due to normal flight-path changes as well as pitch and yaw experienced as the payload precesses. Average or mean values of θ_g and ψ_g due to normal flight-path changes, in addition to the resultant pitch-yaw payload oscillation angle δ_g about these mean values, are illustrated in the following sketch:

APPENDIX



For the deceleration portion of the test $\dot{\theta}_g \ll \dot{\theta}_g$ and $\bar{\psi} \ll \dot{\psi}$, so that angular velocity components about the body axis due to payload oscillations are closely approximated by equations (A3).

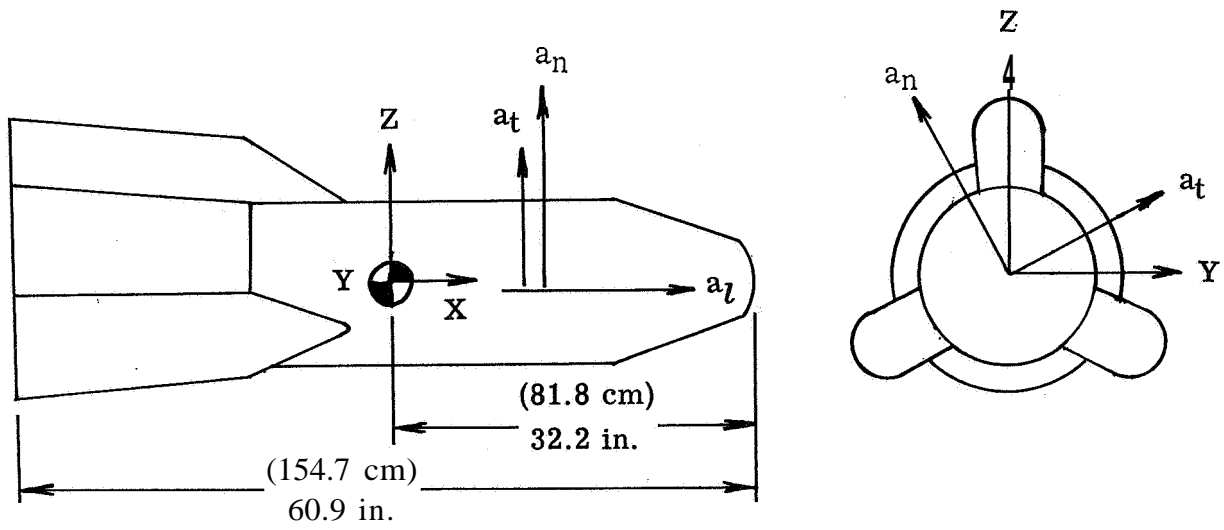
The accelerometers, being located forward of the center of mass of the payload, will contain incremental values of acceleration in their readings as a result of this pitch-yaw oscillation. These accelerations must be subtracted from the accelerometer readings in order to obtain the deceleration of the center of mass caused by the parachute drag force. As found in the literature, these incremental accelerations can be expressed in component form by the following equations:

$$\left. \begin{aligned} a_X &= -(\omega_Y^2 + \omega_Z^2)\Delta X + (\omega_X\omega_Y - \dot{\omega}_Z)\Delta Y + (\omega_X\omega_Z + \dot{\omega}_Y)\Delta Z \\ a_Y &= +(\omega_X\omega_Y + \dot{\omega}_Z)\Delta X - (\omega_X^2 + \omega_Z^2)\Delta Y + (\omega_Y\omega_Z - \dot{\omega}_X)\Delta Z \\ a_Z &= +(\omega_X\omega_Z - \dot{\omega}_Y)\Delta X + (\omega_Y\omega_Z + \dot{\omega}_X)\Delta Y - (\omega_X^2 + \omega_Y^2)\Delta Z \end{aligned} \right\} \quad (A4)$$

Accelerometer designation	AX		AY		AZ	
	in.	cm	in.	cm	in.	cm
Longitudinal	9.72	24.69	0	0	0	0
Transverse	12.10	30.73	.036	.091	.021	.053
Normal	13.34	33.88	-.024	-.061	.041	.104

APPENDIX

The directions of the sensitive **axis** of the accelerometers are shown in the following sketch:



Sketch (3)

REFERENCES

1. McFall, John C., Jr.; and Murrow, Harold N.: Parachute Testing at Altitudes Between 30 and 90 Kilometers. **AIAA** Aerodynamic Deceleration Systems Conference, Sept. 1966, pp. 116-121.
2. Whitlock, Charles H.; Bendura, Richard J.; and Coltrane, Lucille C.: Performance of a 26-Meter-Diameter Ringsail Parachute in a Simulated Martian Environment. NASA TM X-1356, 1967.
3. Thiele, Otto W.: Density and Pressure Profiles Derived From Meteorological Rocket Measurements. Tech. Rept. 108, Missile Meteorol. Div., U.S. Army Signal Missile Support Agency, Sept. 1961. (Available From DDC as AD 263546.)

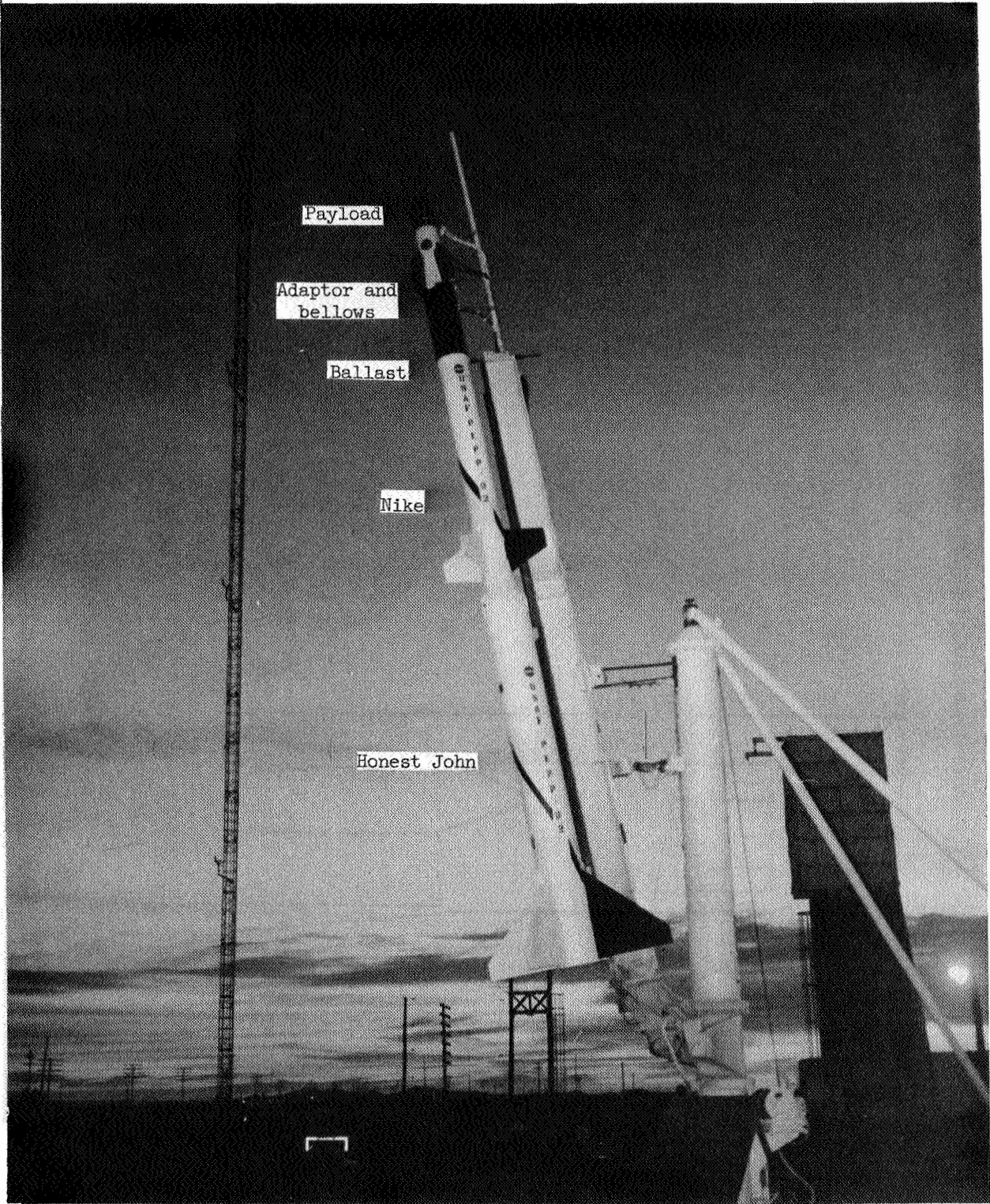


Figure 1- Photograph of vehicle configuration. U.S. Army photograph.

L-67-1083

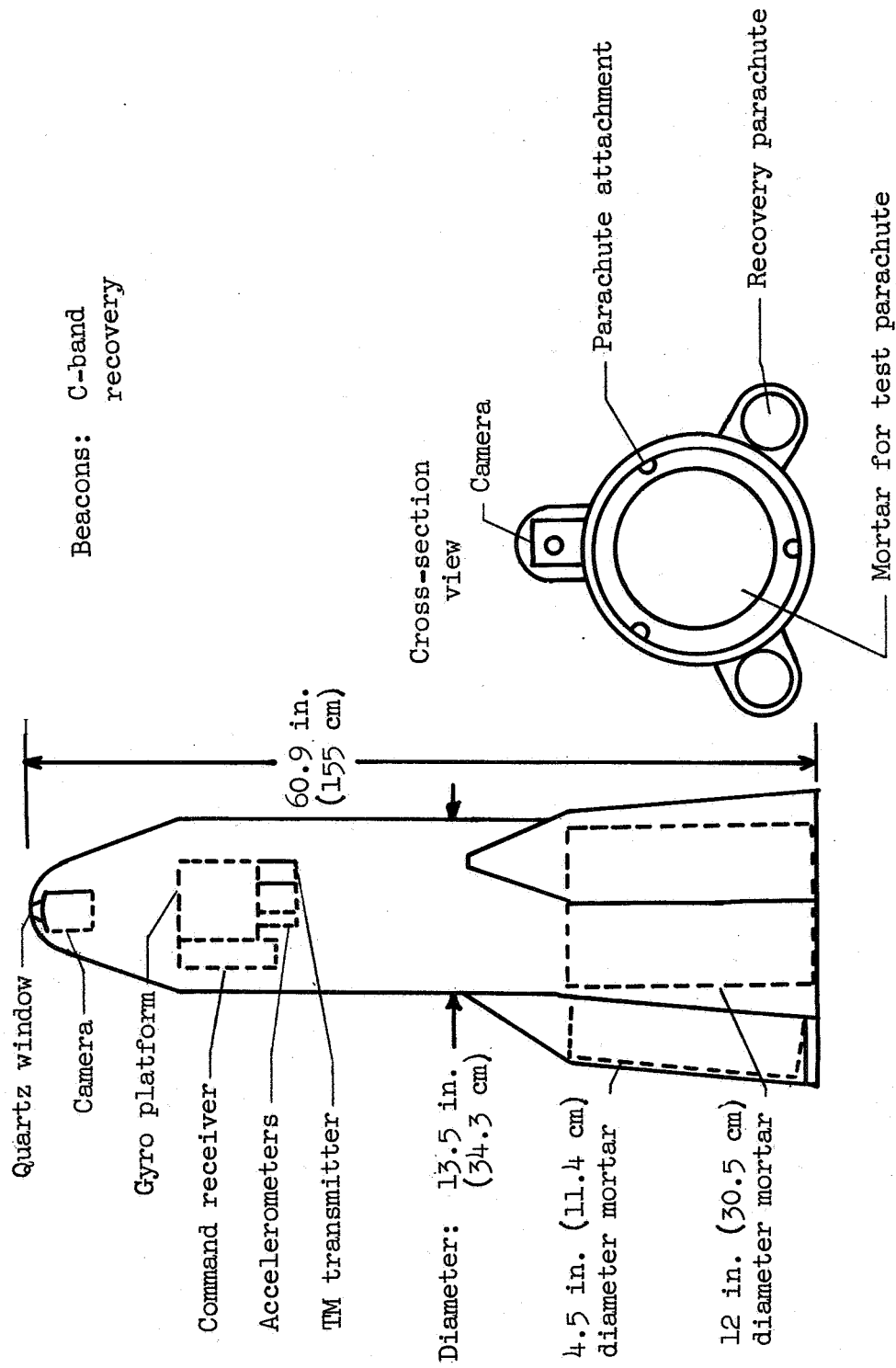


Figure 2.- Test payload.

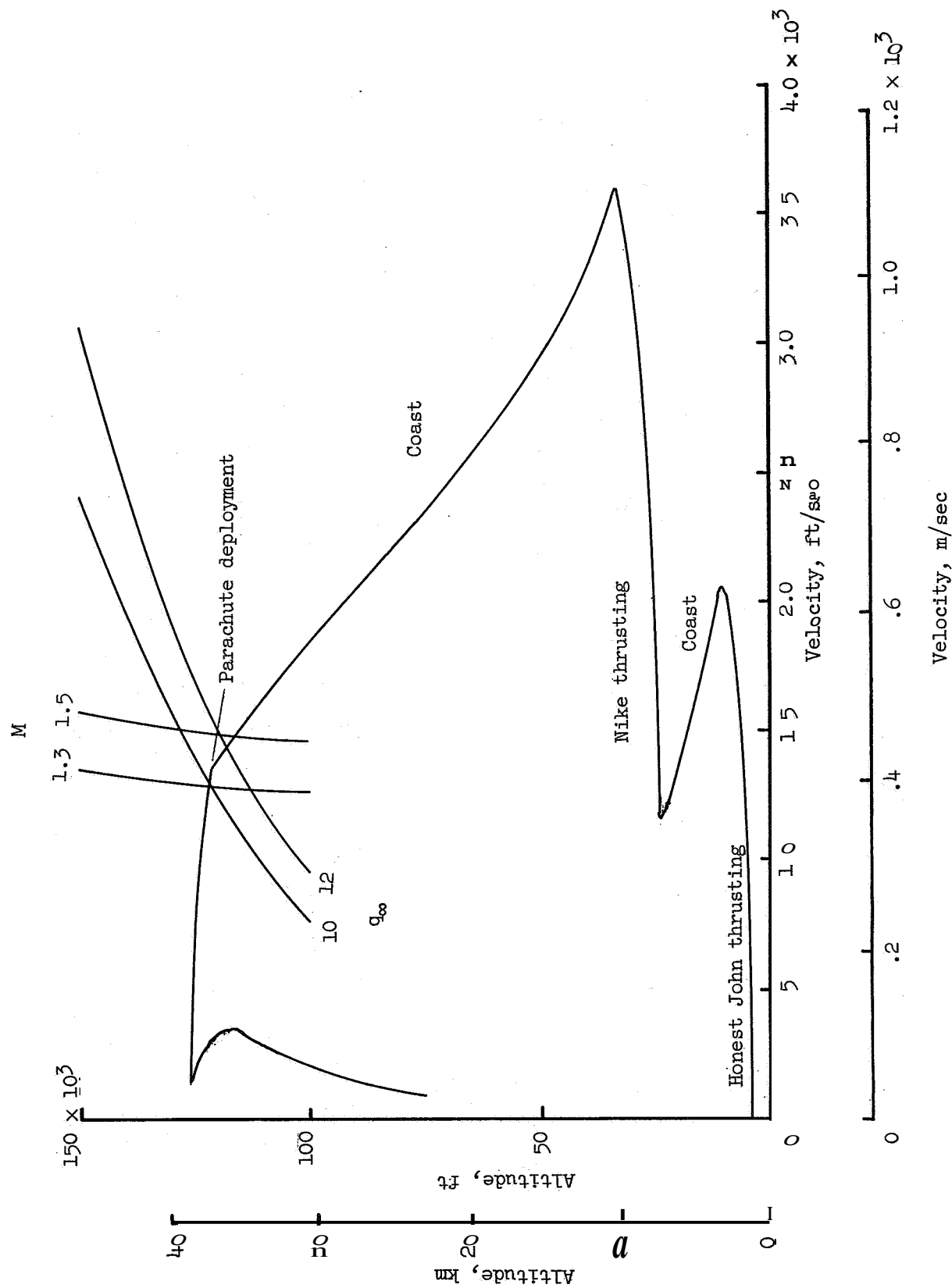
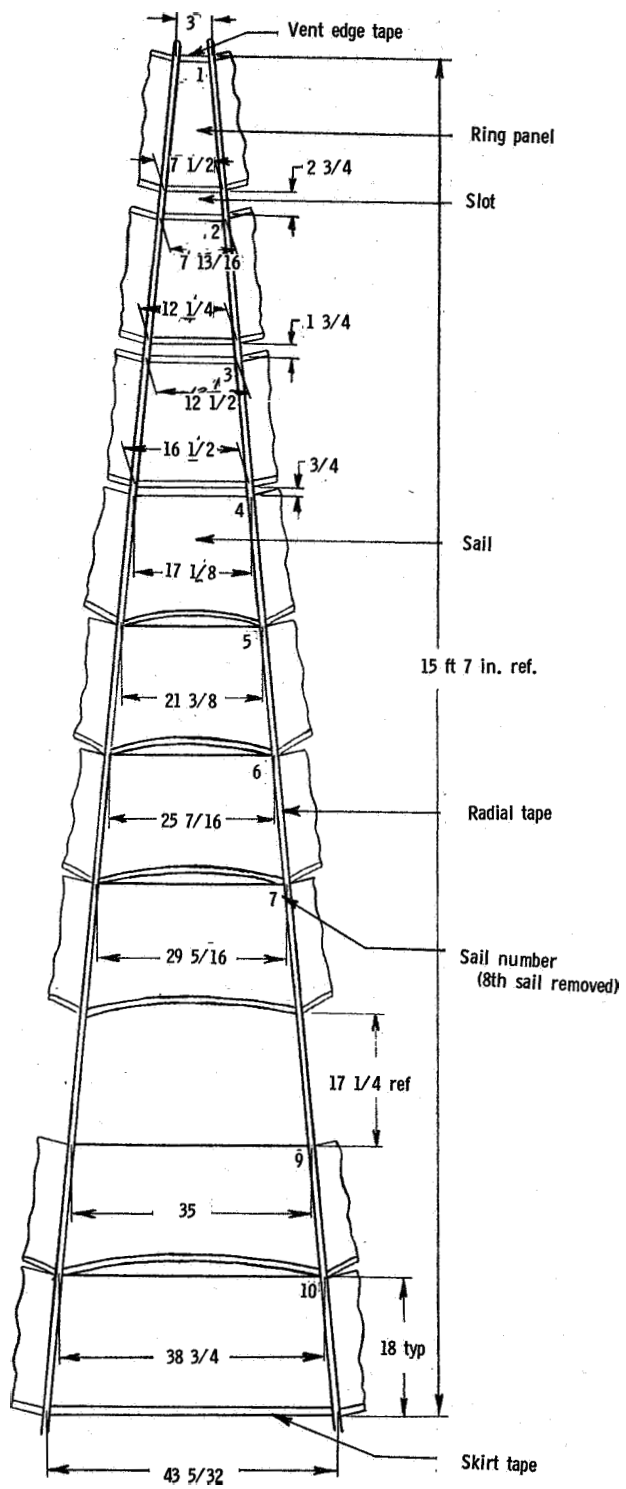
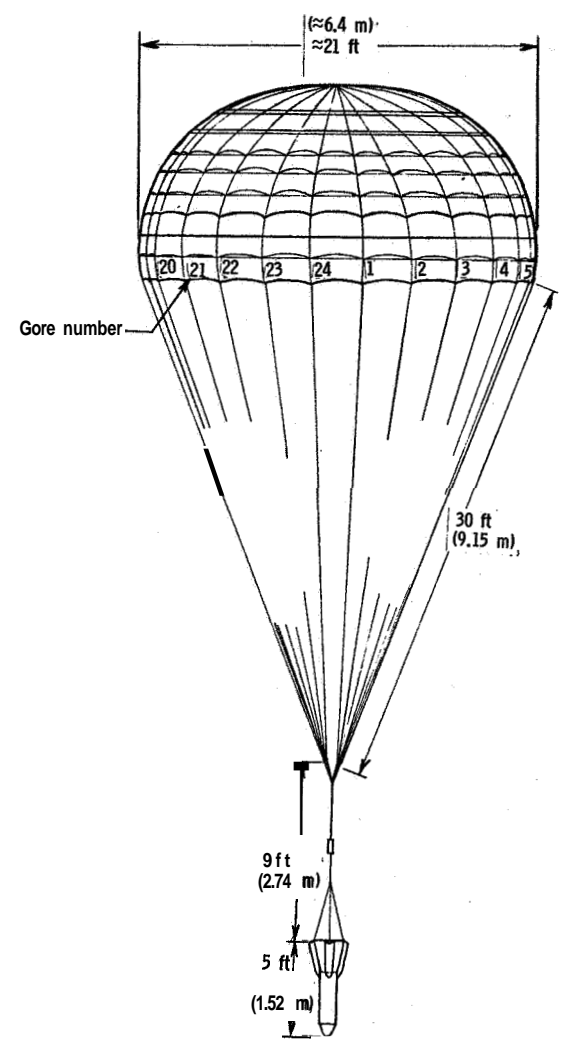


Figure 3.- Visual display for command deployment.

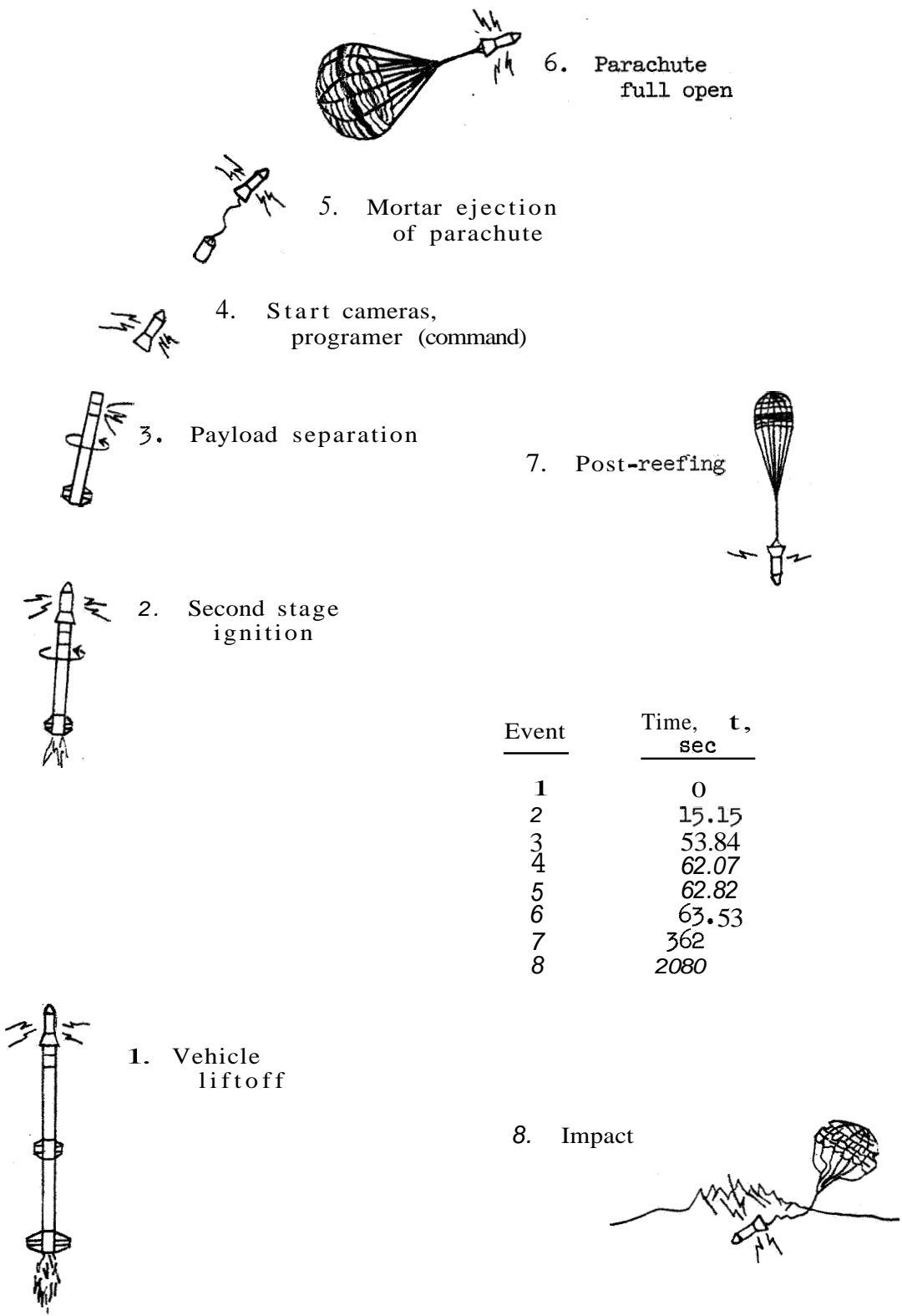


Gore dimensional details



Flight configuration

Figure 4.- Ringsail parachute-gore dimensional details and flight configuration.



6. Parachute full open

5. Mortar ejection of parachute

4. Start cameras, programmer (command)

3. Payload separation

7. Post-reefing

2. Second stage ignition

Event	Time, t , sec
1	0
2	15.15
3	53.84
4	62.07
5	62.82
6	63.53
7	362
8	2080

1. Vehicle liftoff

8. Impact

Figure 5- Flight sequence of event.

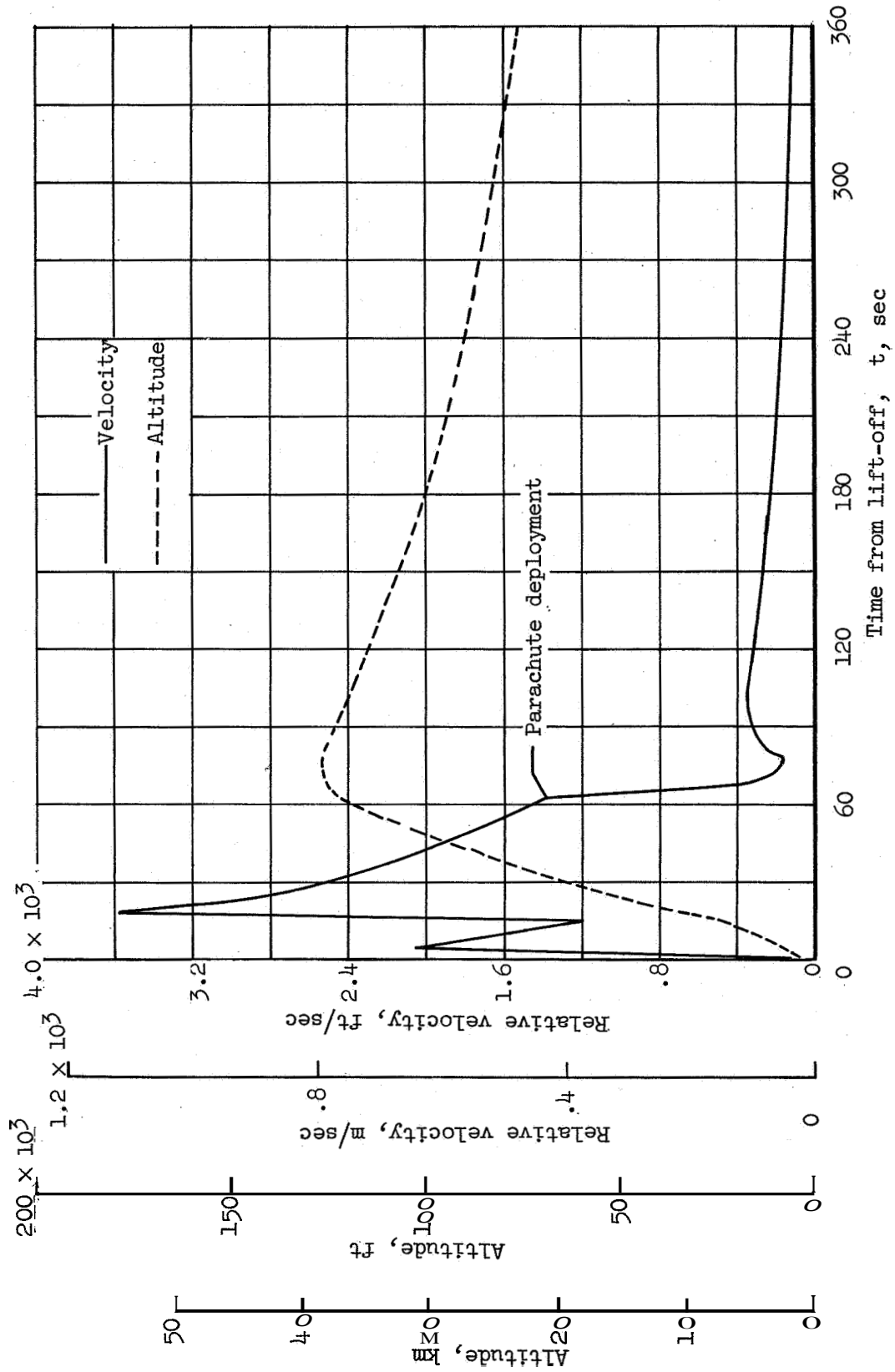


Figure 6.- Time histories of altitude and relative velocity.

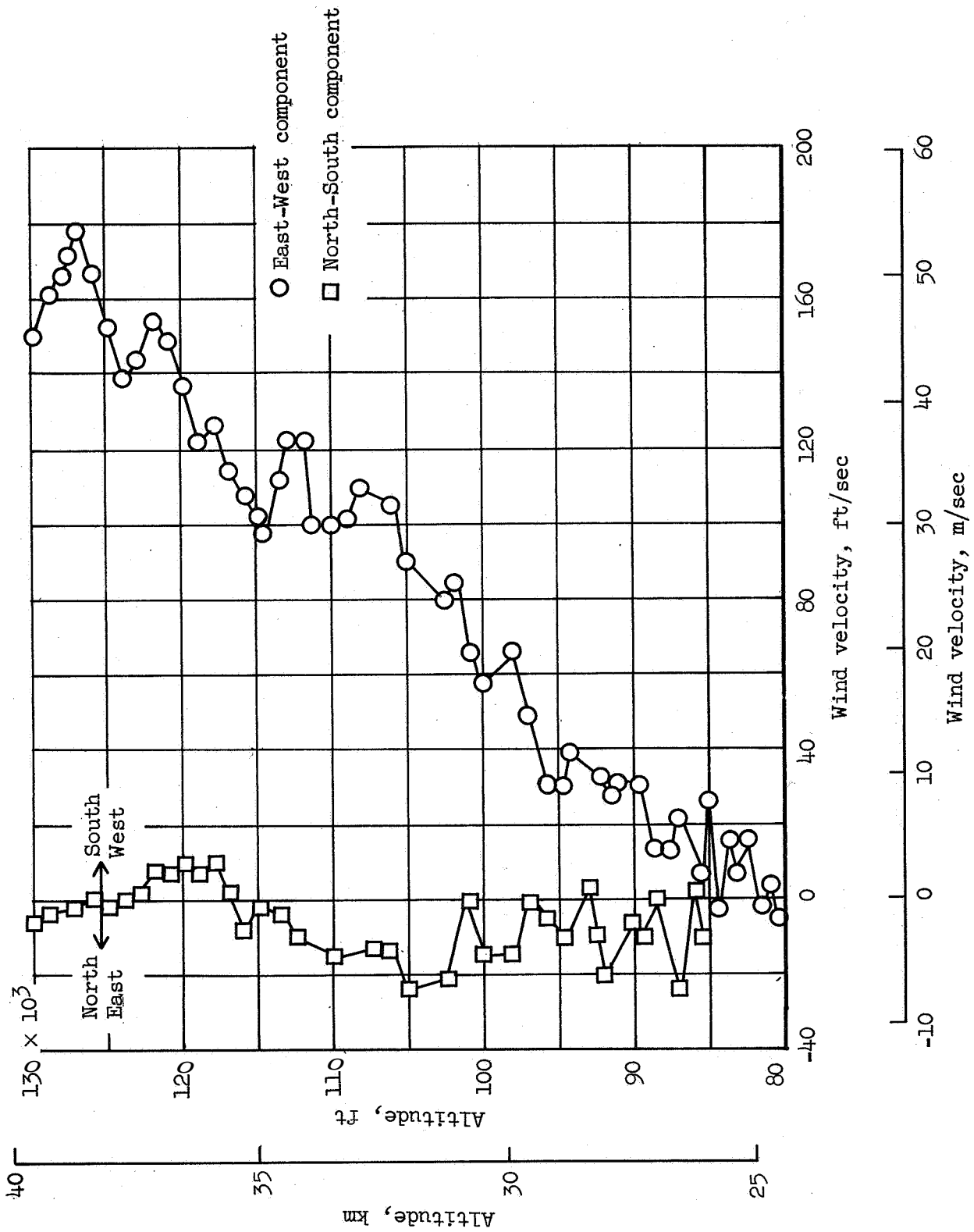


Figure 7.- Wind-velocity profile in east-west and north-south components.

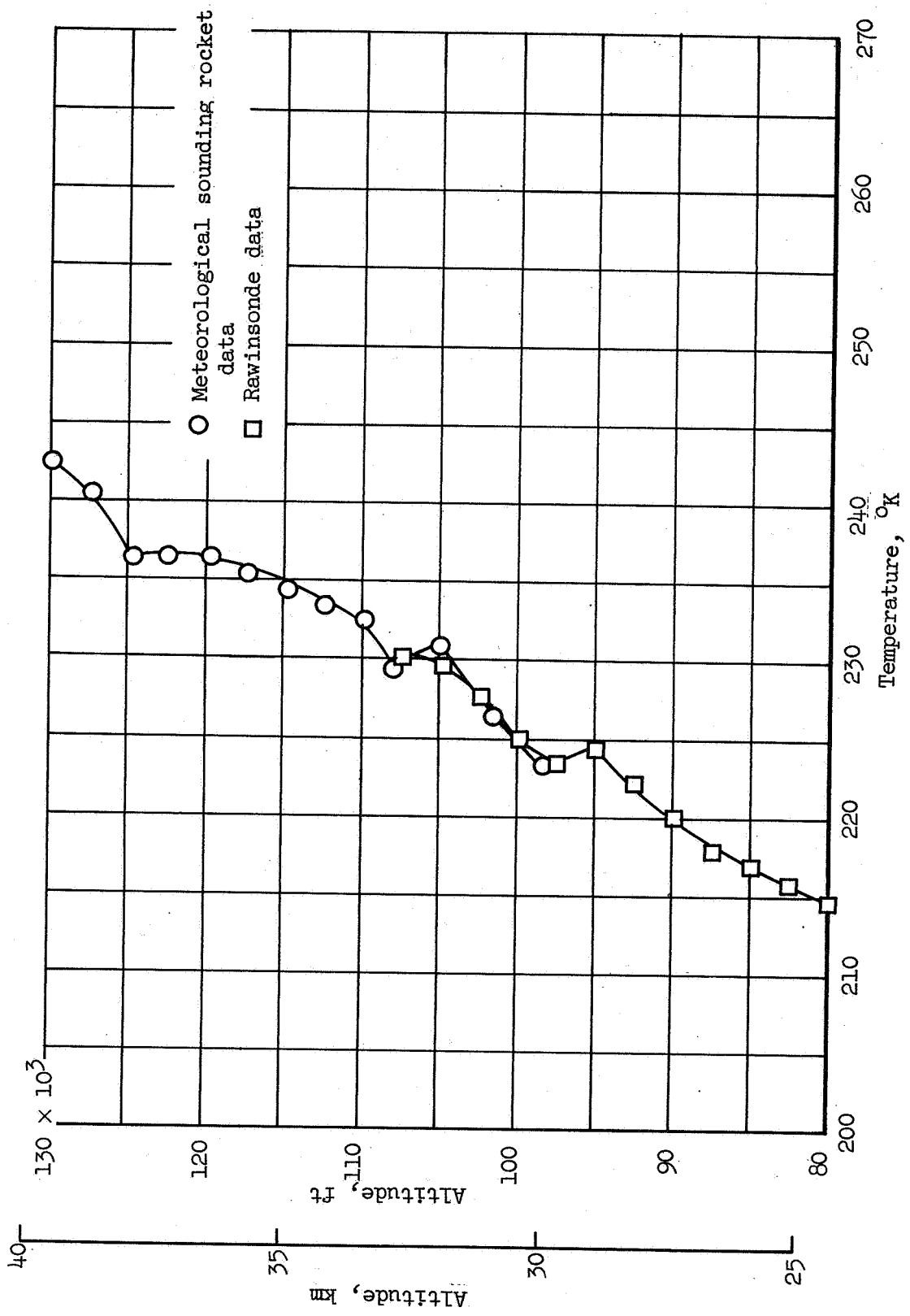


Figure 8.- Atmospheric temperature profile.

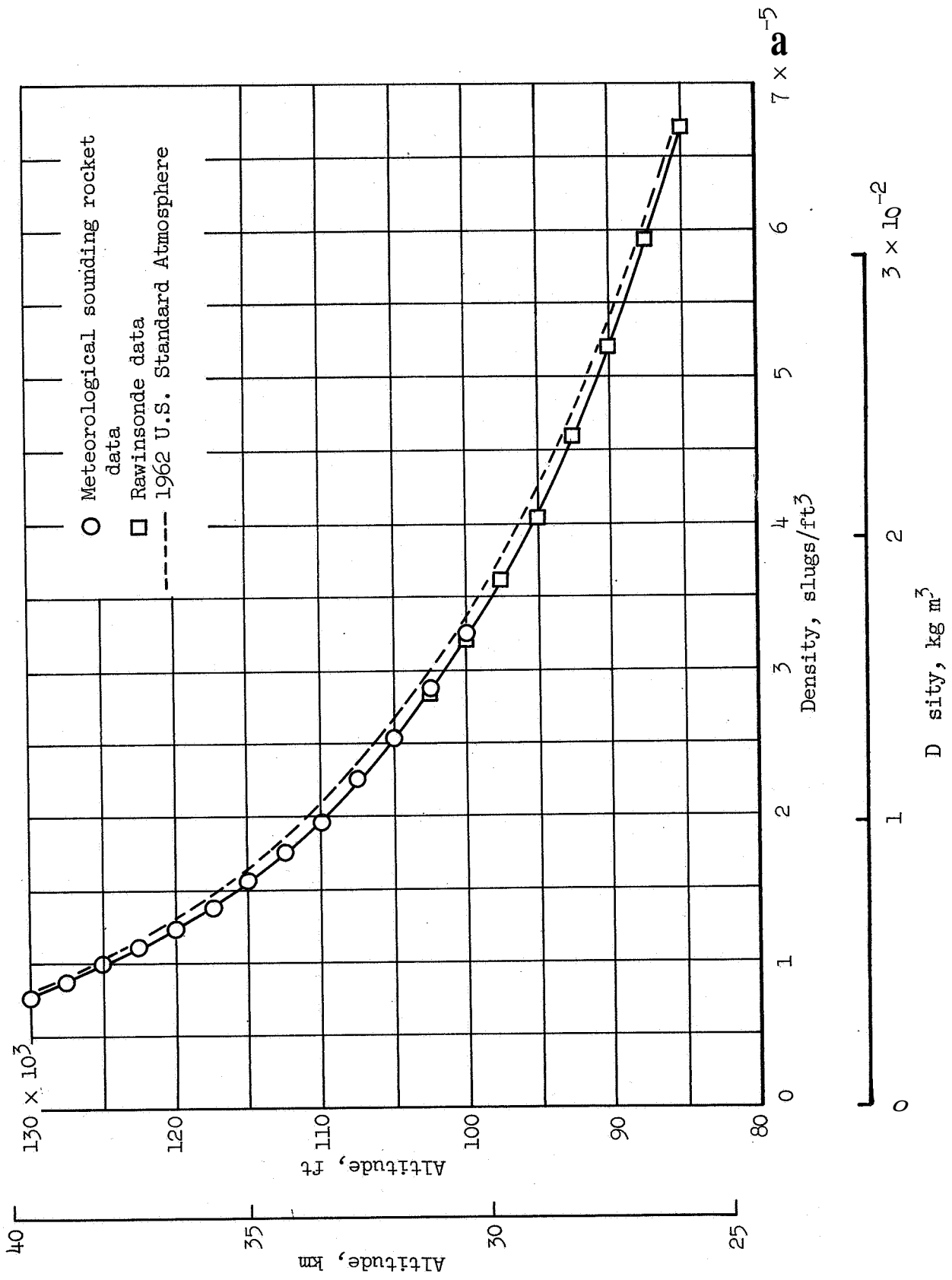


Figure 9.- Atmospheric density profile.

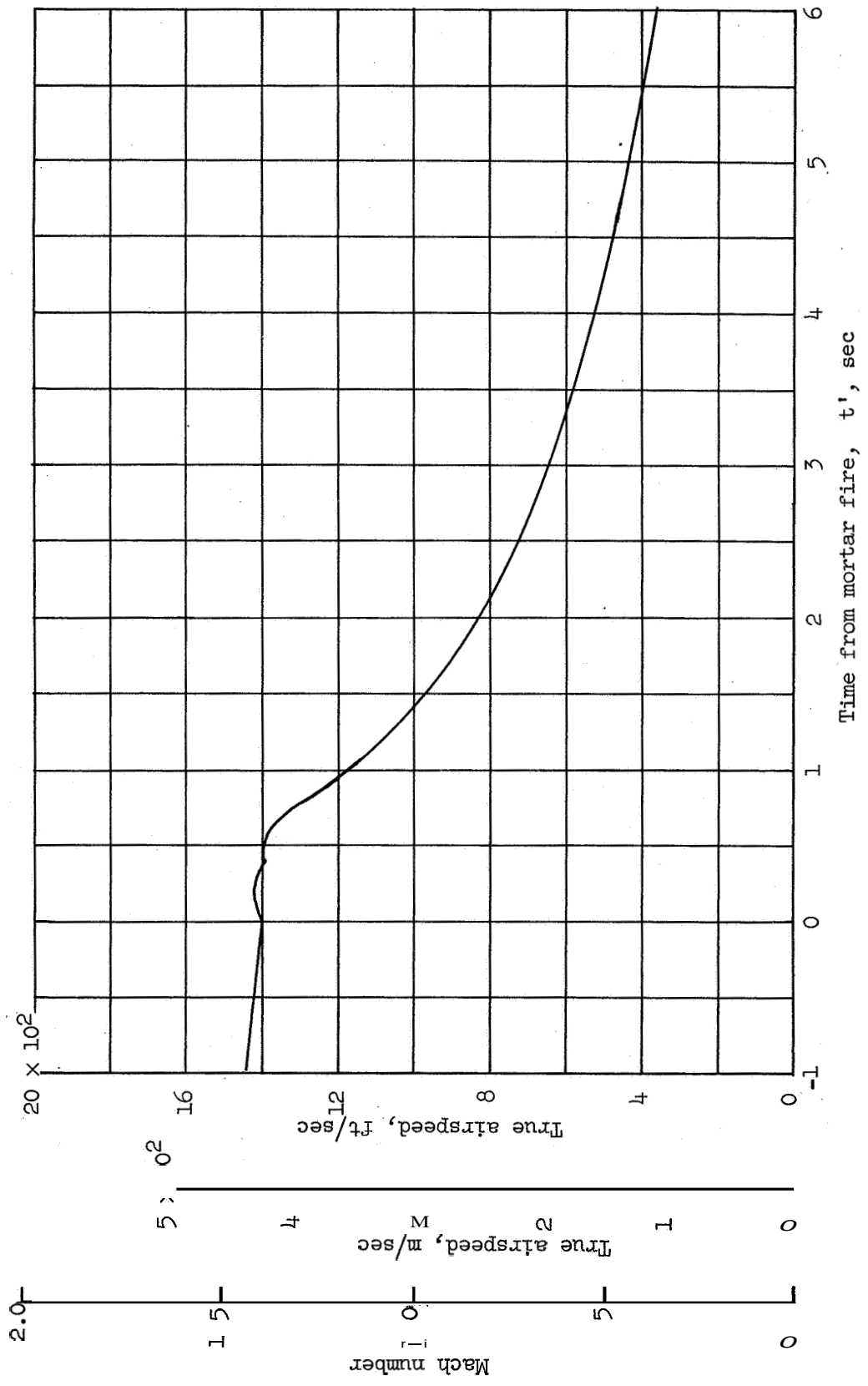
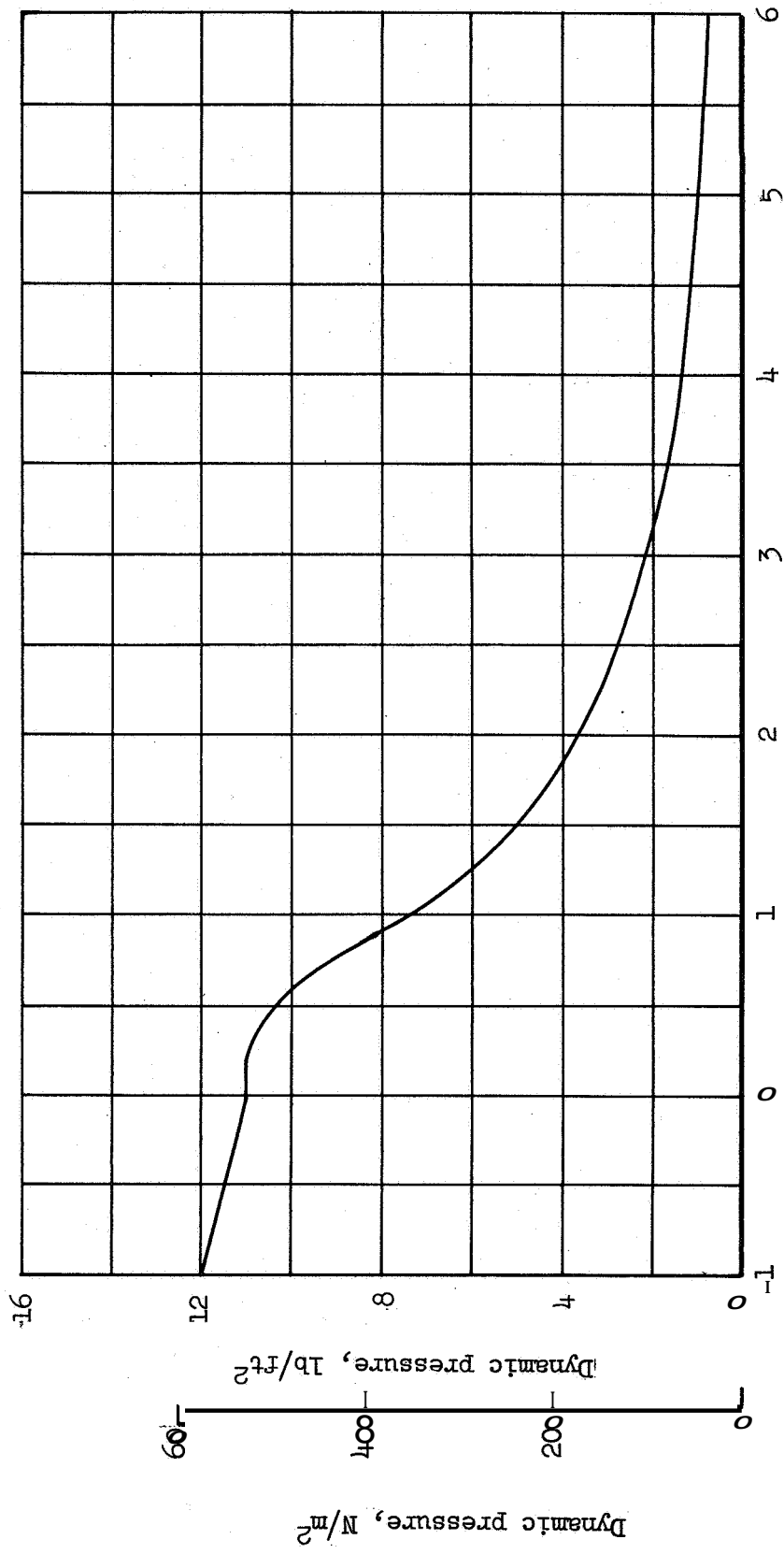
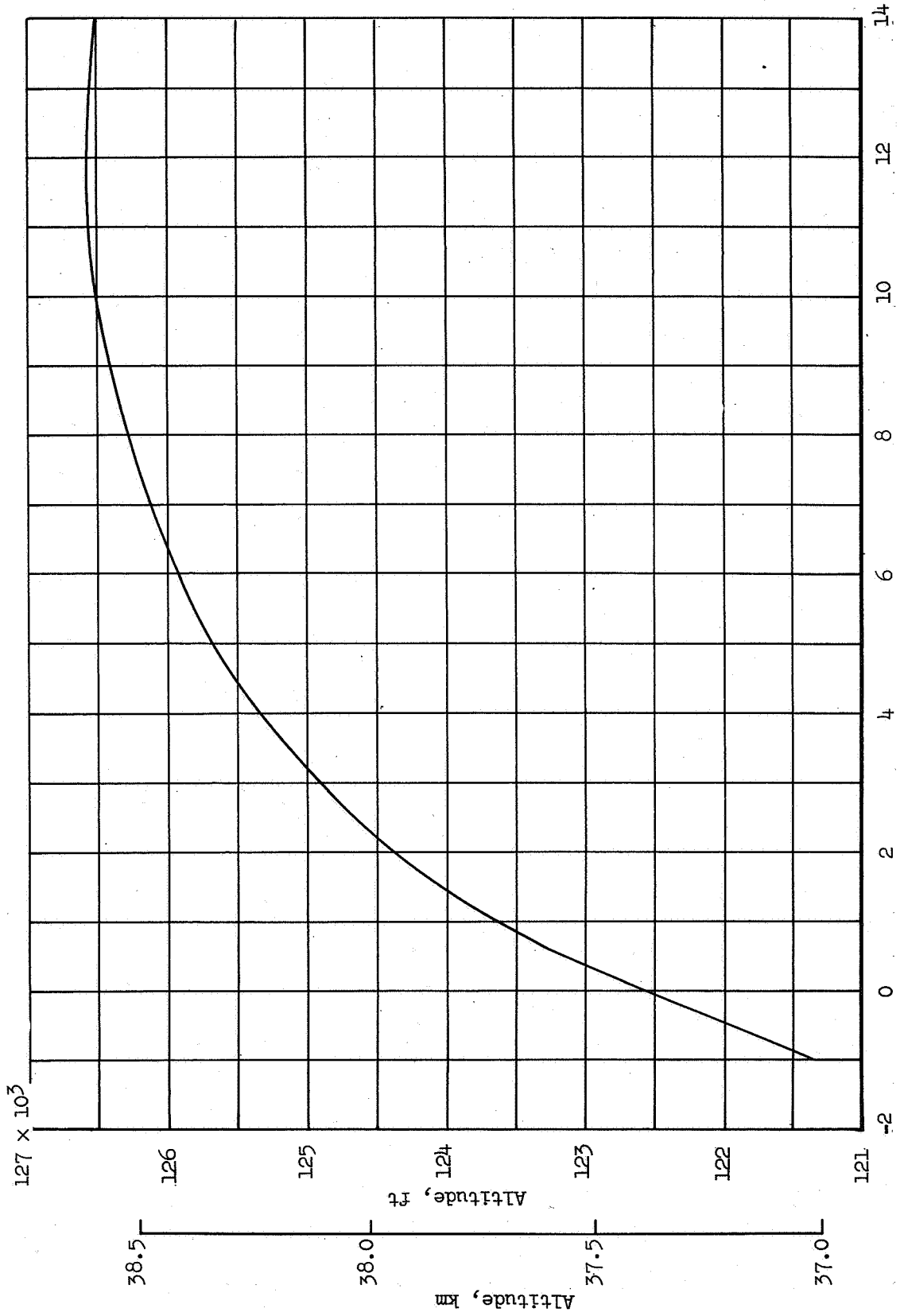


Figure 10.- Mach number and true airspeed time histories.



Time from mortar fire, t , sec

Figure 11.- Dynamic pressure time history.



Time from mortar fire, t', sec

Figure 12.- Altitude time history.

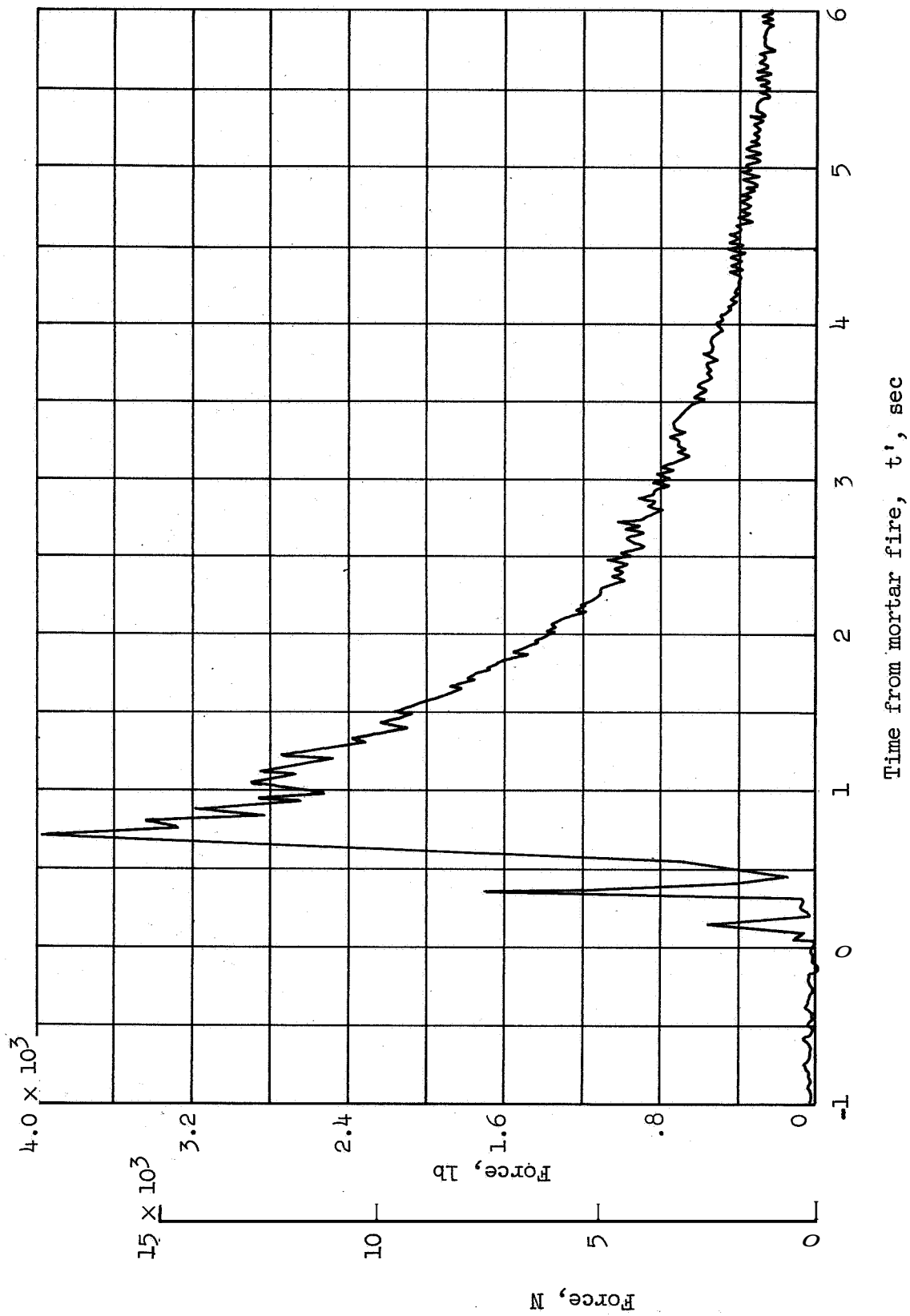


FIG 13.- Tensiometer face time history.

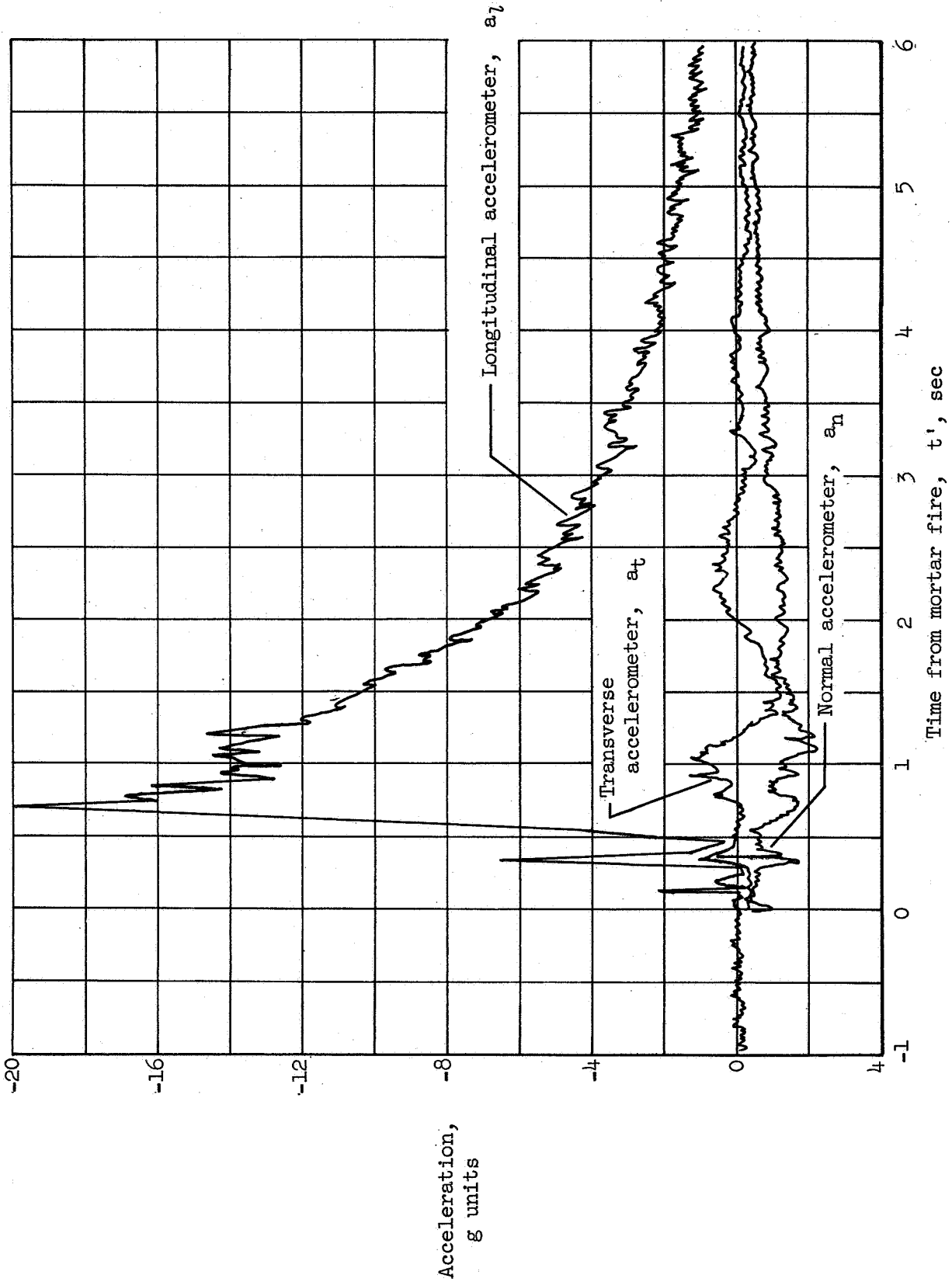
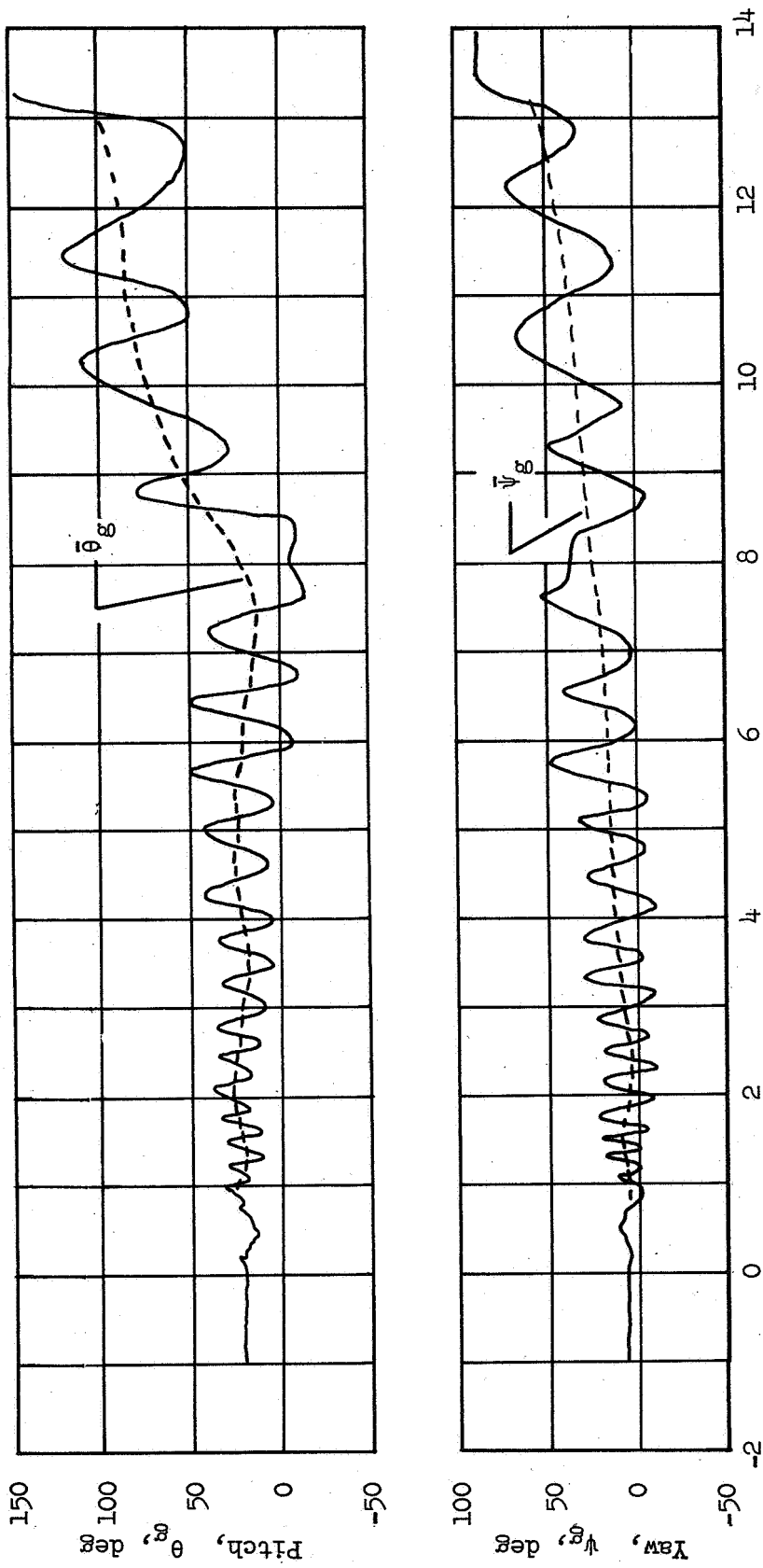
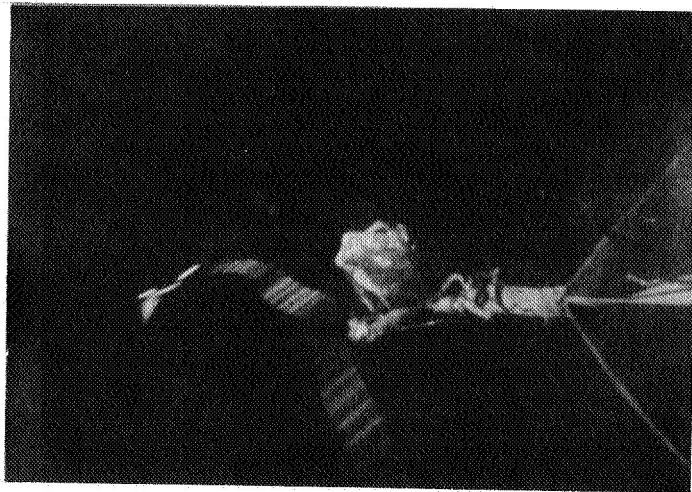


Figure 14.- Acceleration time histories.

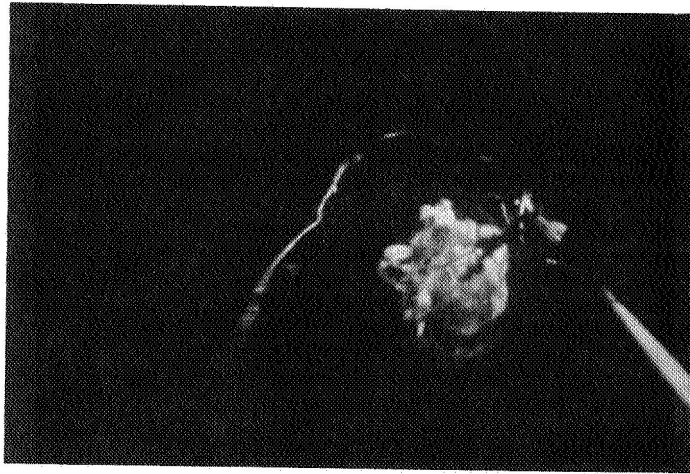


Time from mortar fire, t' , sec

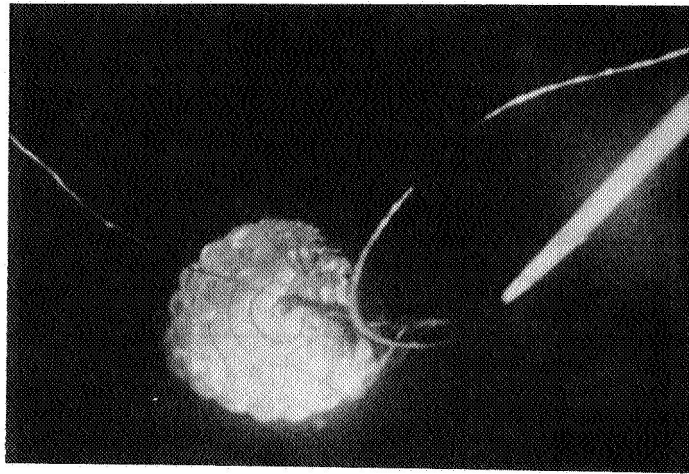
Figure 15.- Payload pitch and yaw time histories. Pitch down is positive.



$t' = 0.45 \text{ sec}$



$t' = 0.50 \text{ sec}$

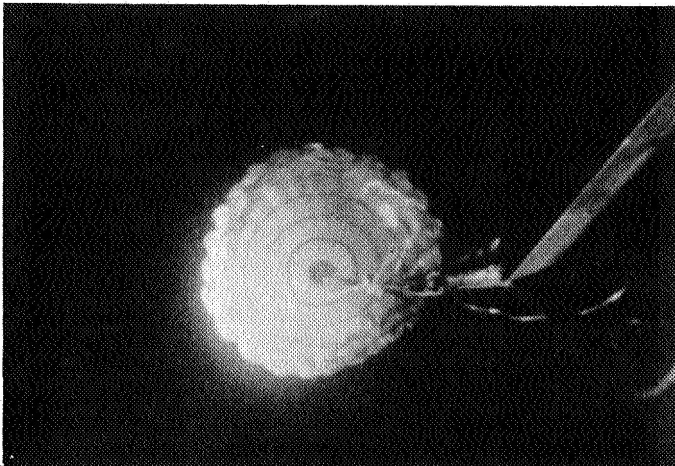


$t' = 0.58 \text{ sec}$

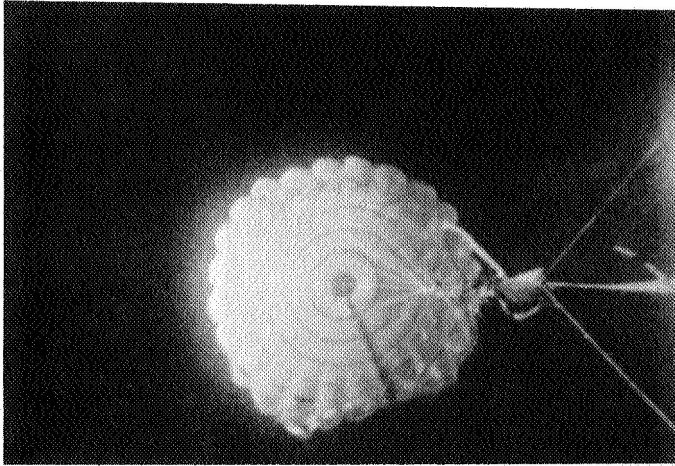
(a) Canopy inflation.

Figure 16.- Onboard membrane photographs.

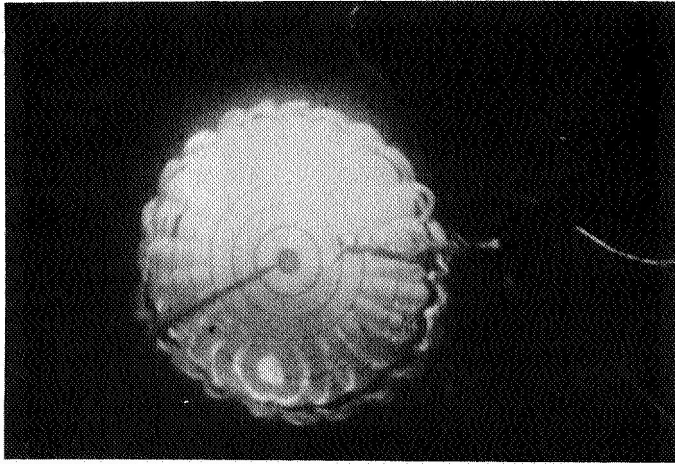
L-67 1087



$t' = 0.63 \text{ sec}$



$t' = 0.66 \text{ sec}$

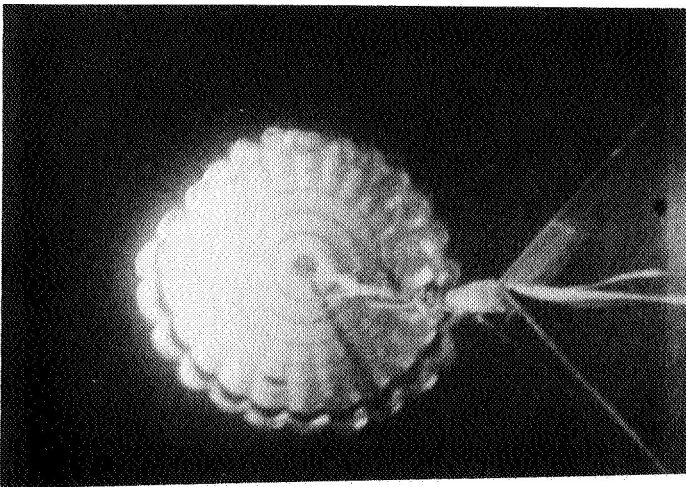


$t' = 0.70 \text{ sec}$

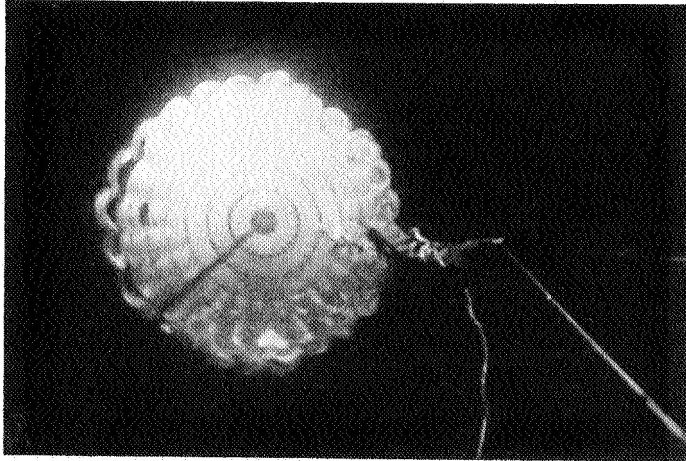
(a) Concluded.

Figure 16.- Continued.

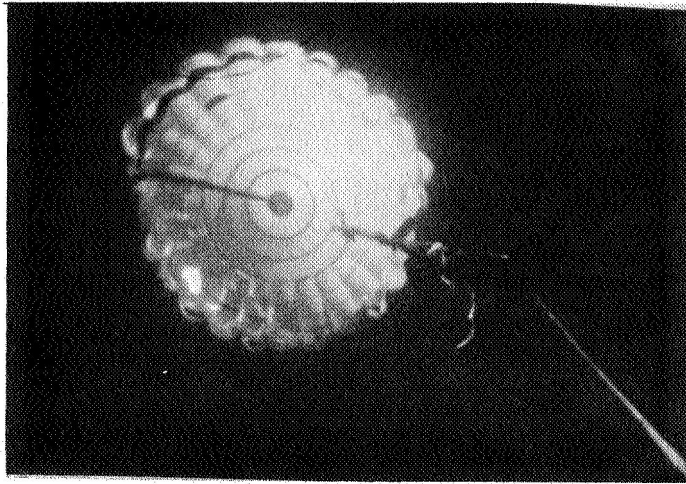
L-67-1086



$t' = 0.86 \text{ sec}$



$t' = 0.91 \text{ sec}$

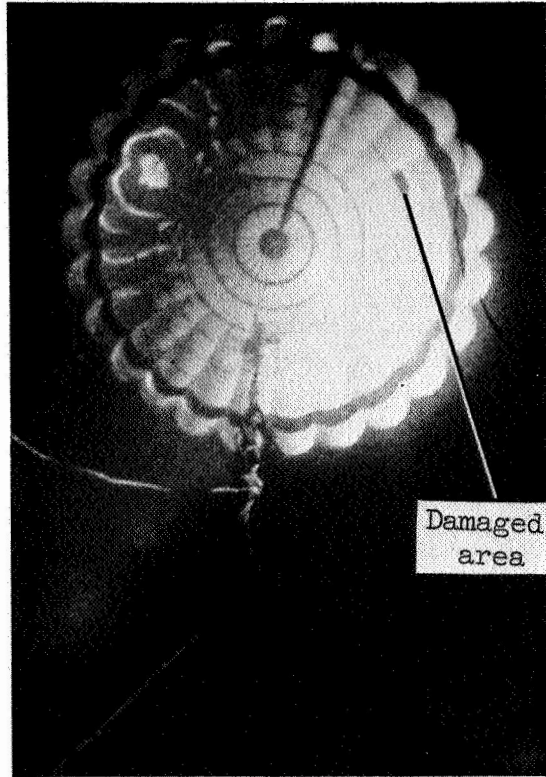


$t' = 0.94 \text{ sec}$

(b) Flutter of canopy kite.

Figure 16.- Continued.

L-67-1085



$t' = 2.00 \text{ sec}$

(c) Stable inflation. I-67-1084

Figure 16- Concluded.

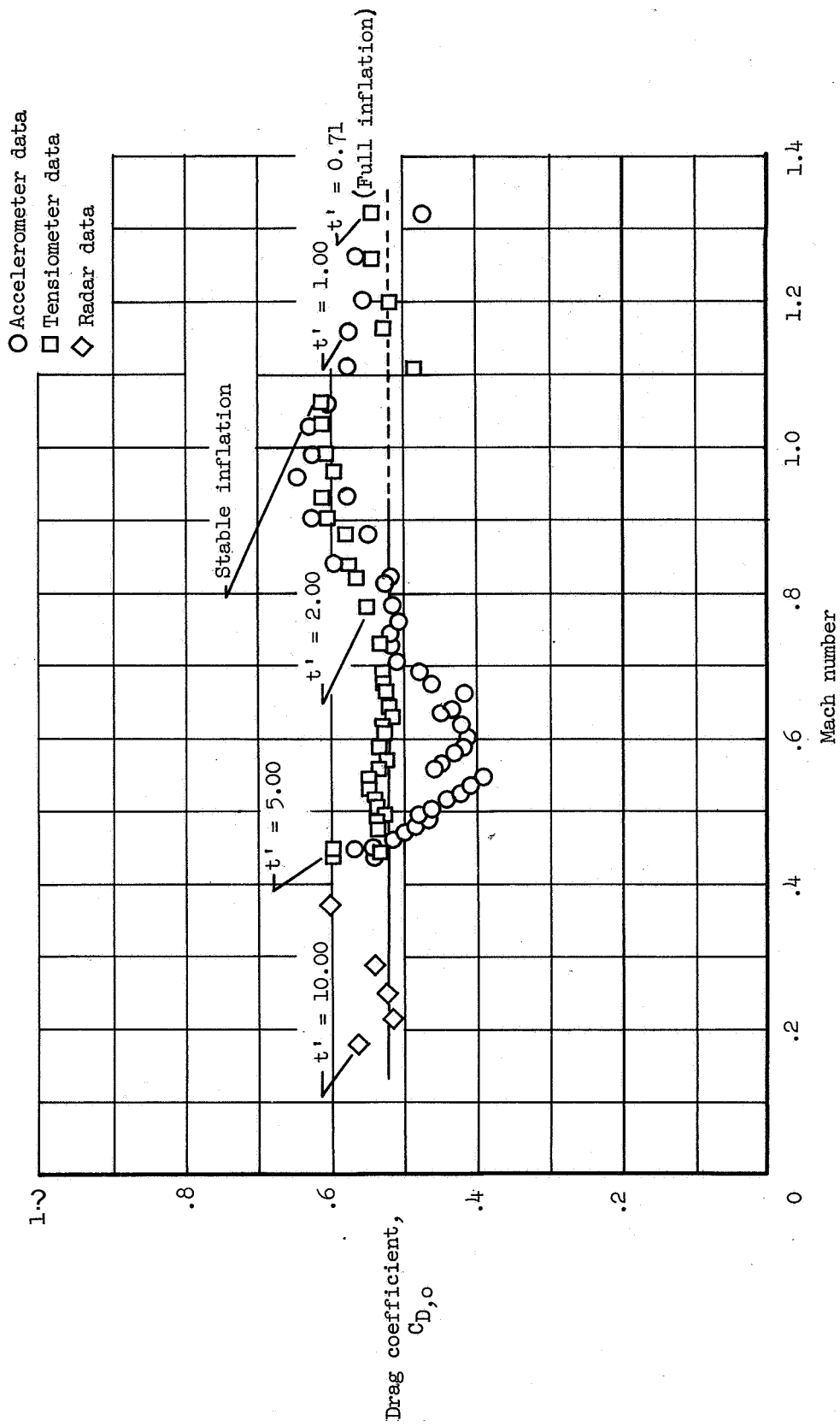


Figure 17.- Variation of parachute drag coefficient with Mach number.

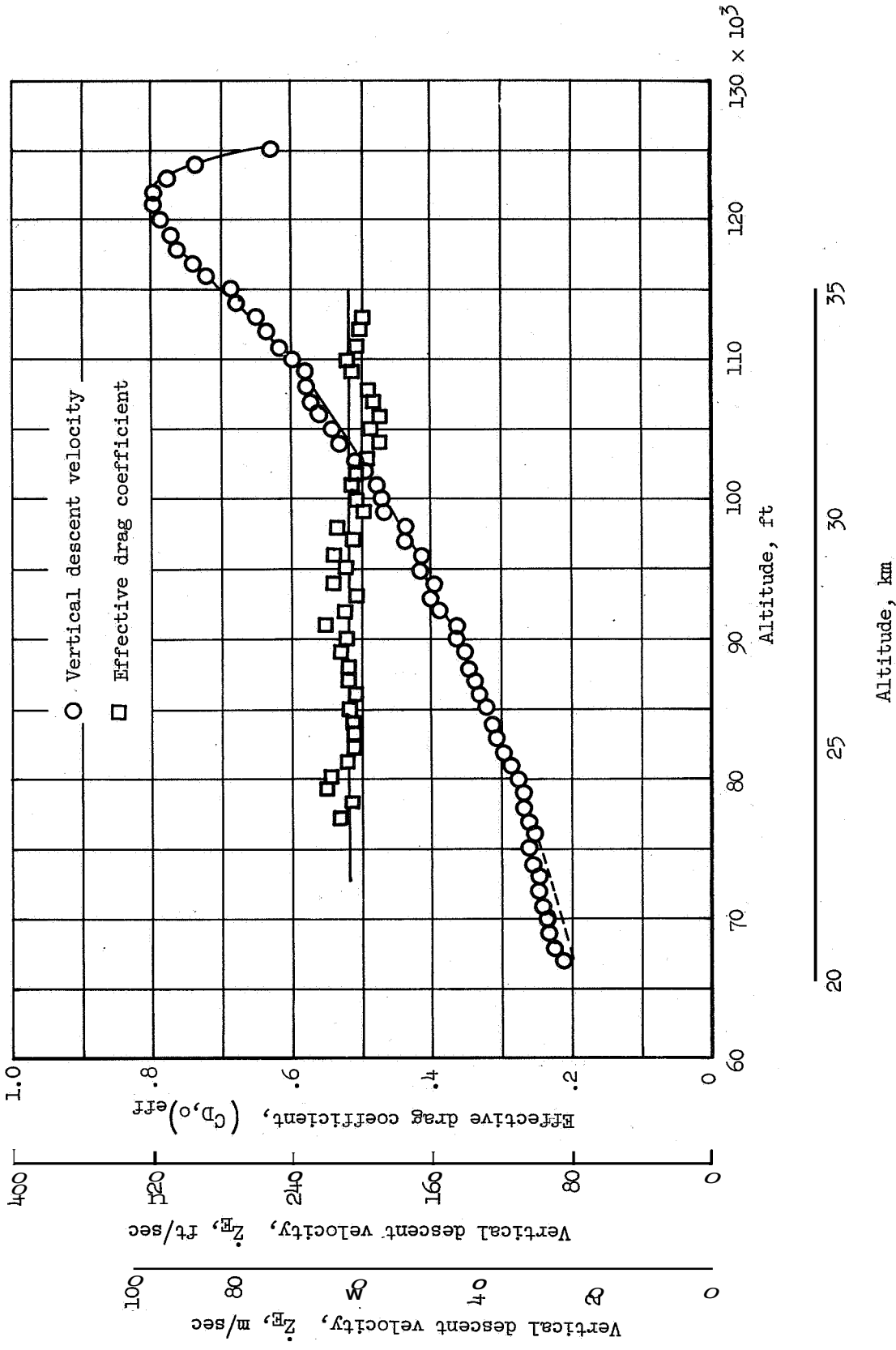


Figure 18.- Variation of vertical descent velocity and effective drag coefficient with altitude.

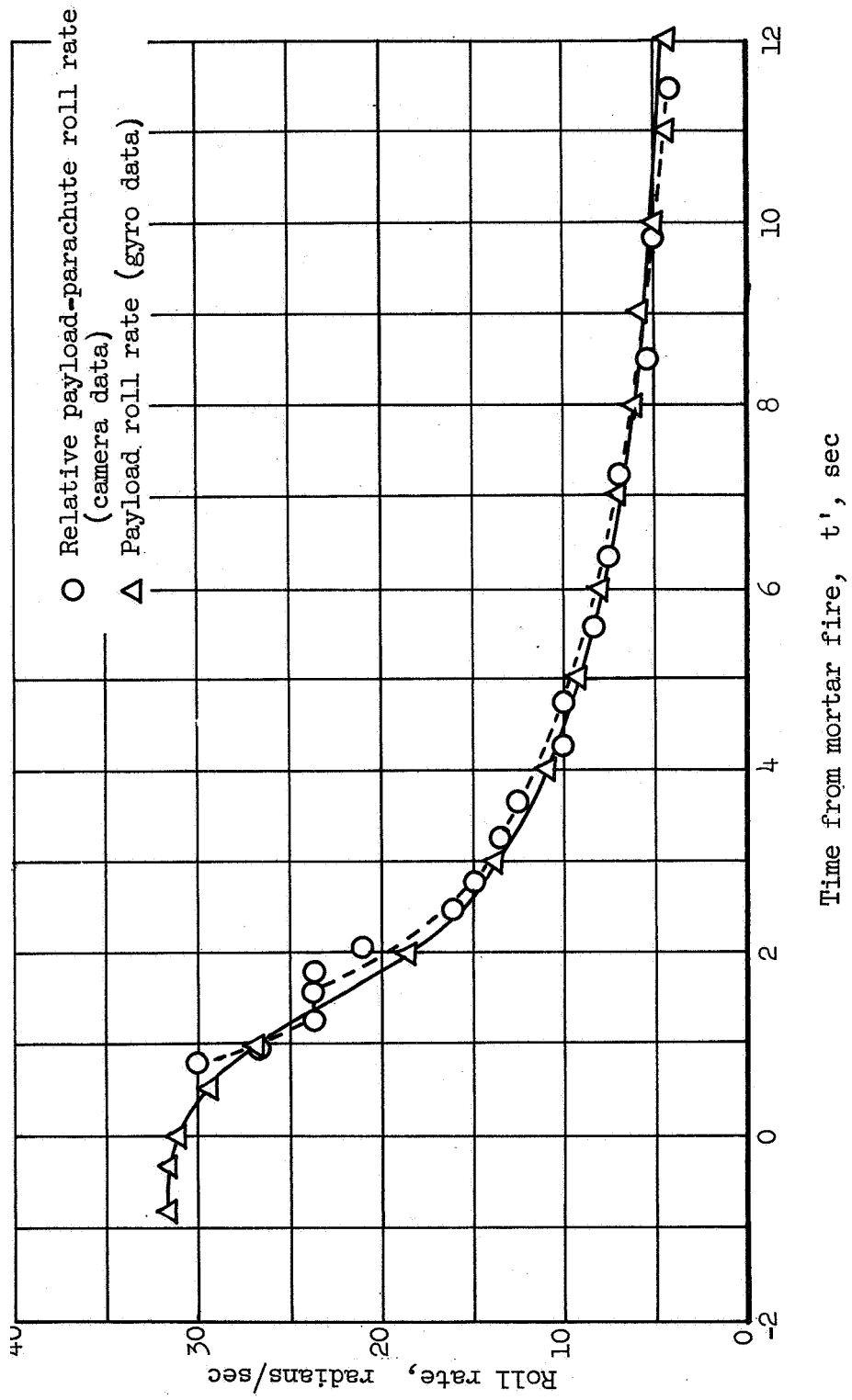


Figure 19.- Comparison of payload roll rate with relative payload-parachute roll rate.

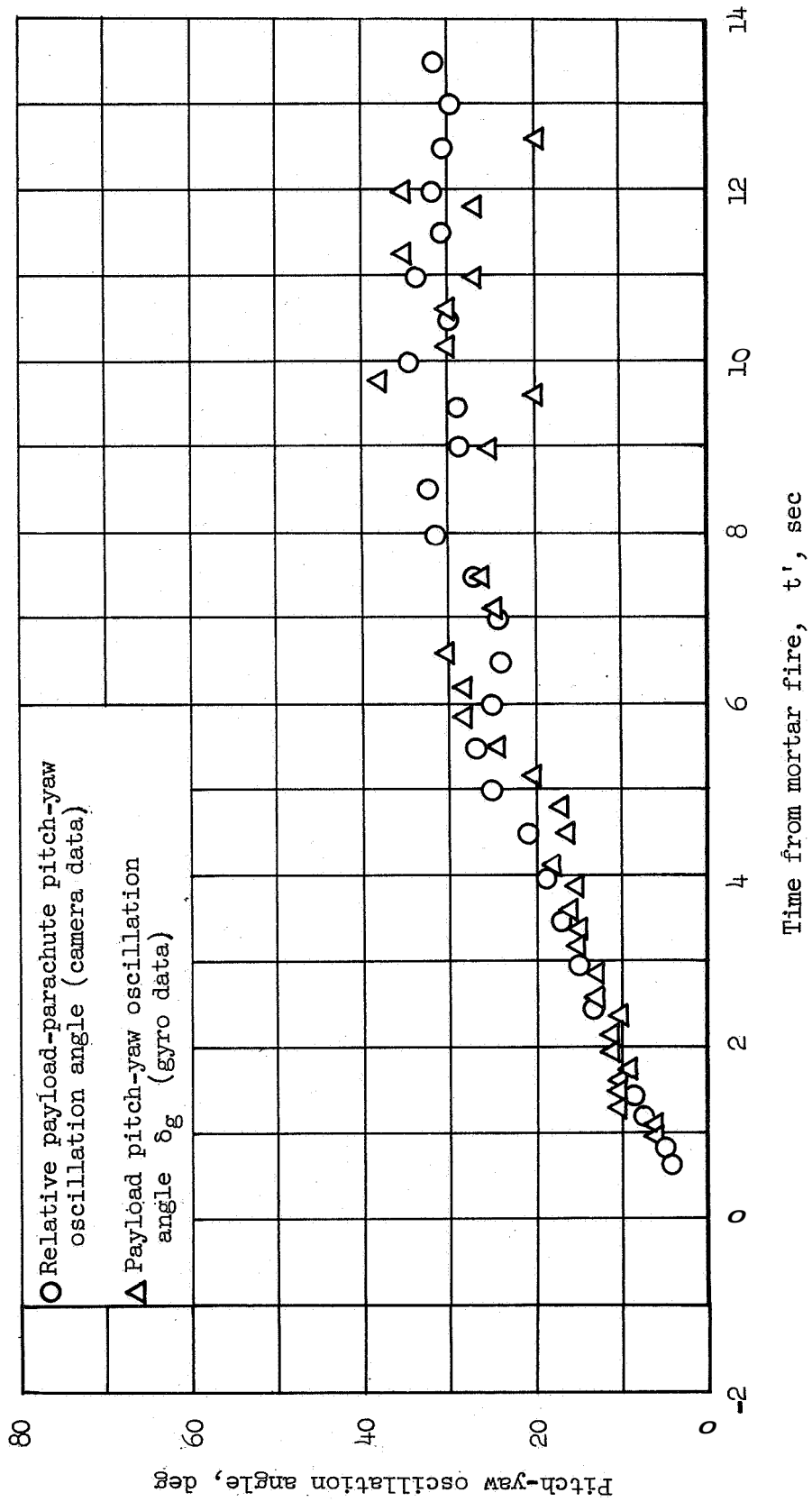


Figure 20.- Comparison of payload pitch-yaw oscillation angle with relative payload-parachute pitch-yaw oscillation angle.

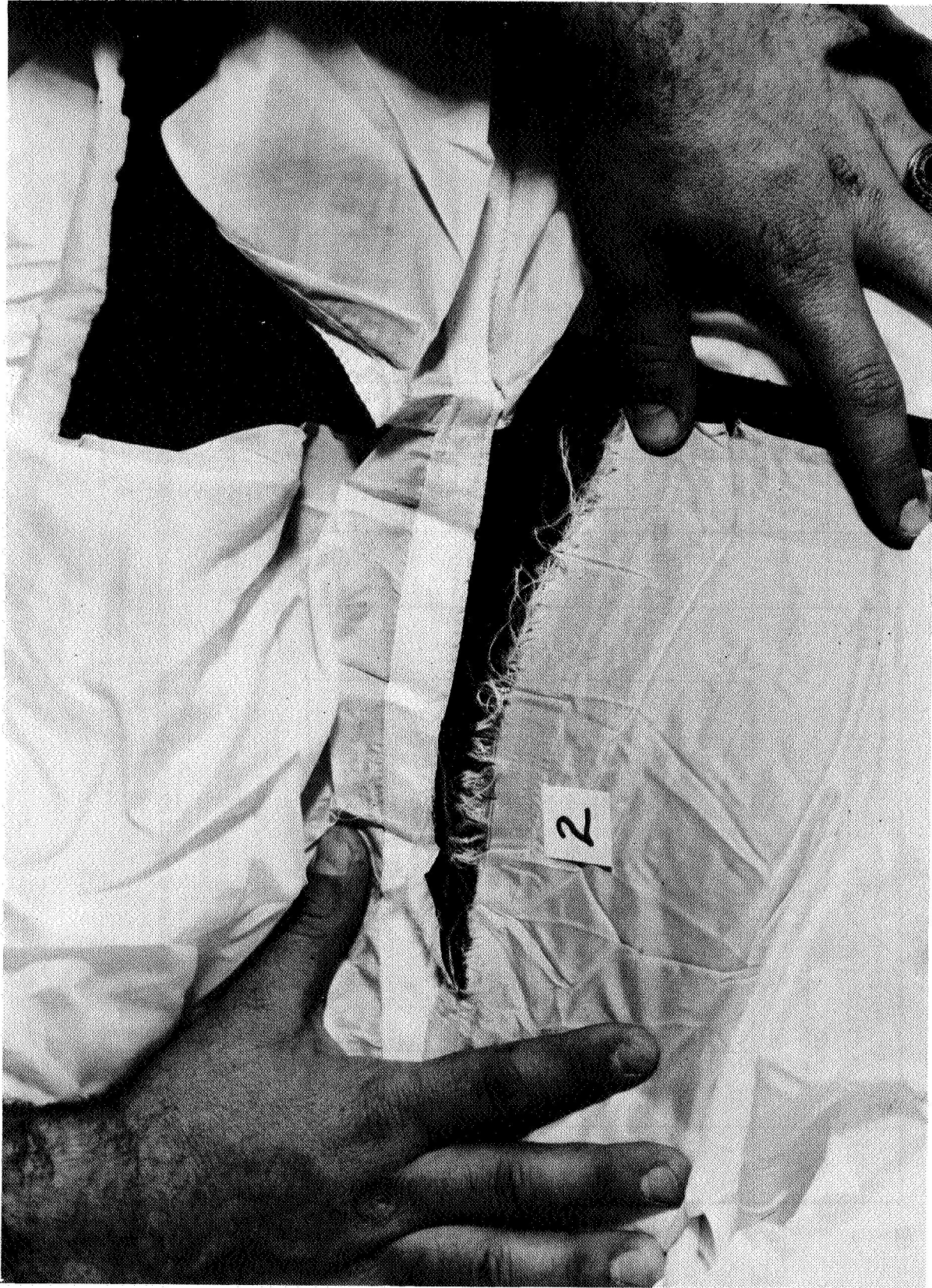


Figure 21.- Photograph of EMB with maximum damage.

L-66-9676

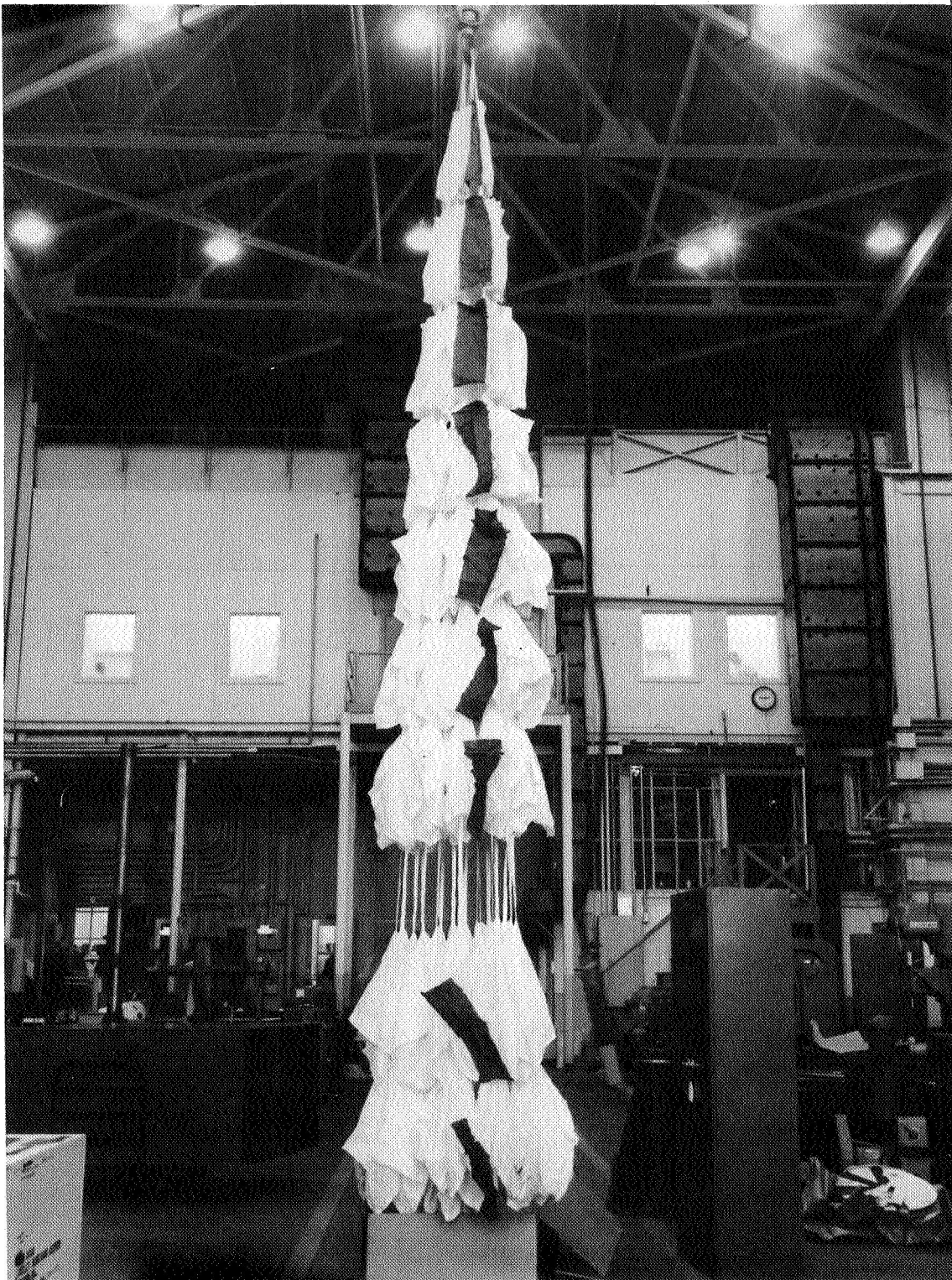


Figure 22.- Photograph of recovered parachute.

L-66-9691

"The aeronautical and space activities of the United States shall be conducted so as to contribute . . . to the expansion of human knowledge of phenomena in the atmosphere and space. The Administration shall provide for the widest practicable and appropriate dissemination of information concerning its activities and the results thereof."

—NATIONAL AERONAUTICS AND SPACE ACT OF 1958

NASA SCIENTIFIC AND TECHNICAL PUBLICATIONS

TECHNICAL REPORTS: Scientific and technical information considered important, complete, and a lasting contribution to existing knowledge.

TECHNICAL NOTES: Information less broad in scope but nevertheless of importance as a contribution to existing knowledge.

TECHNICAL MEMORANDUMS: Information receiving limited distribution because of preliminary data, security classification, or other reasons.

CONTRACTOR REPORTS: Scientific and technical information generated under a NASA contract or grant and considered an important contribution to existing knowledge.

TECHNICAL TRANSLATIONS: Information published in a foreign language considered to merit NASA distribution in English.

SPECIAL PUBLICATIONS: Information derived from or of value to NASA activities. Publications include conference proceedings, monographs, data compilations, handbooks, sourcebooks, and special bibliographies.

TECHNOLOGY UTILIZATION PUBLICATIONS: Information on technology used by NASA that may be of particular interest in commercial and other non-aerospace applications. Publications include Tech Briefs, Technology Utilization Reports and Notes, and Technology Surveys.

Details on the availability of these publications may be obtained from:

SCIENTIFIC AND TECHNICAL INFORMATION DIVISION
NATIONAL AERONAUTICS AND SPACE ADMINISTRATION

Washington, D.C. 20546